EJN fens European Journal of Neuroscience

European Journal of Neuroscience, Vol. 28, pp. 1808–1824, 2008 doi:10.1111/j.1460-9568.2008.06473.x

NEUROSYSTEMS

Neutralization of the membrane protein Nogo-A enhances growth and reactive sprouting in established organotypic hippocampal slice cultures

Luis M. Craveiro,[1,2] David Hakkoum,[3] Oliver Weinmann,[1] Laura Montani,[1] Luc Stoppini[4] and Martin E. Schwab[1]
[1]Brain Research Institute, University of Zurich, Zurich, Switzerland
[2]Department of Biology, Swiss Federal Institute of Technology, Zurich, Switzerland
[3]Department of Basic Neurosciences, University of Geneva, Geneva, Switzerland
[4]Capsant Neurotechnologies Limited, Biomedical Sciences Building, Bassett Crescent East, Southampton, UK

Keywords: axonal growth, growth inhibition, plasticity, sprouting, transcriptomics

Abstract

The reduced ability of central axons to regenerate after injury is significantly influenced by the presence of several molecules that inhibit axonal growth. Nogo-A is one of the most studied and most potent of the myelin-associated growth inhibitory molecules. Its neutralization, as well as interference with its signalling, allows for enhanced axonal sprouting and growth following injury. Using differentiated rat organotypic hippocampal slice cultures treated for 5 days with either of two different function-blocking anti-Nogo-A antibodies, we show an increase in CA3 fibre regeneration after lesion. In intact slices, 5 days of anti-Nogo-A antibody treatment led to increased sprouting of intact CA3 fibres that are positive for neurofilament 68. A transcriptomic approach confirmed the occurrence of a growth response on the molecular level upon Nogo-A neutralization in intact cultures. Our results demonstrate that Nogo-A neutralization for 5 days is sufficient for the induction of growth in mature CNS tissue without the prerequisite of an injury. Nogo-A may therefore act as a tonic growth suppressor/stabilizer in the adult intact hippocampus.

Introduction

Adult CNS lesions often have devastating consequences due to the low regeneration and structural repair capacity of the tissue. This phenomenon can partly be explained by the presence of neurite outgrowth inhibitory molecules (Filbin, 2006; Benowitz & Yin, 2007). Nogo-A, one of the most potent growth inhibitors of the adult CNS and the first one being discovered (Caroni & Schwab, 1988; Chen *et al.*, 2000), has been extensively studied.

Nogo-A signals via the receptor complex NgR/p75/Lingo-1/Troy (Fournier *et al.*, 2001; Wang *et al.*, 2002; Mi *et al.*, 2004; Park *et al.*, 2005) and an as yet unidentified Nogo-A-specific receptor (Niederost *et al.*, 2002; Dodd *et al.*, 2005). Two active sites, Nogo-66 and a Nogo-A-specific region, lead to activation of RhoA and ROCK (Niederost *et al.*, 2002; Fournier *et al.*, 2003; Schweigreiter *et al.*, 2004; Hsieh *et al.*, 2006; McKerracher & Higuchi, 2006), thereby affecting the neuronal growth machinery.

In rats with stroke lesions, Nogo-A neutralization (Papadopoulos *et al.*, 2002, 2006; Emerick *et al.*, 2003), or blockade of NgR (Lee *et al.*, 2004), allowed compensatory fibre sprouting and functional innervation from the intact side to the denervated side of the spinal cord and brainstem. Similar results were also observed in spinal cord-lesioned rats and monkeys treated with anti-Nogo-A antibodies (Schnell & Schwab, 1990; Merkler *et al.*, 2001; Schwab, 2004; Liebscher *et al.*, 2005; Freund *et al.*, 2006), in rats infused with NgR antagonist peptides (GrandPre *et al.*, 2002) or an activity-blocking receptor fragment (Li *et al.*, 2004), and in Nogo-A (Kim *et al.*, 2003; Simonen *et al.*, 2003; Dimou *et al.*, 2006) or NgR (Kim *et al.*, 2004) knockout mice.

The Nogo-A function in the intact CNS tissue is poorly understood. Its neutralization *in vivo* produced a transitory growth response of Purkinje axons and of the corticospinal tract in intact adult rats (Buffo *et al.*, 2000; Bareyre *et al.*, 2002; Gianola *et al.*, 2003). In adulthood, Nogo-A is highly expressed in oligodendrocytes and some neurons of the hippocampus (Huber *et al.*, 2002; Meier *et al.*, 2003; Gil *et al.*, 2006; Trifunovski *et al.*, 2006). This expression has been shown to decline with age (Trifunovski *et al.*, 2006). Organotypic hippocampal slice cultures are a commonly used *in vitro* model to study hippocampal function and structure (Stoppini *et al.*, 1991, 1993; Bahr, 1995; Gahwiler *et al.*, 1997; Hakkoum *et al.*, 2007). They mature *in vitro* and retain many *in vivo* features from a structural and functional perspective. We chose this model to study the role of Nogo-A in the intact adult hippocampus. We analysed the effects of acute Nogo-A neutralization, using two Nogo-A-specific function-blocking monoclonal antibodies, 11C7 and 7B12 (Oertle *et al.*, 2003; Wiessner *et al.*, 2003; Liebscher *et al.*, 2005). Both in the presence and absence of a lesion, we observed induced growth responses morphologically and

Correspondence: Dr L. M. Craveiro, [1]Brain Research Institute, as above.
E-mail: craveiro@hifo.unizh.ch

Received 26 July 2007, revised 26 August 2008, accepted 28 August 2008

biochemically in differentiated cultures treated with antibodies for only 5 days. Notably, no undesirable effects, e.g. spontaneous epileptic activity after Nogo-A neutralization, have been observed.

Materials and methods

Organotypic hippocampal slice cultures and anti-Nogo-A antibody treatment

Hippocampal slices were cultured as previously described (Stoppini *et al.*, 1991). Briefly, Wistar rats (bred in house) were decapitated and their hippocampi were dissected and immediately cut into 350-μm thick slices. Slices were separated in ice-cold dissecting medium, and then four slices were placed into a Millicel-CM insert (Millipore, MA, USA) with 1 mL of culture medium and placed into six-well plates (TPP, Switzerland). Cultures were kept for 21 days at 33°C, in a 5% CO_2 atmosphere. Mouse monoclonal antibody 11C7, directed against rat aa 623–640 of Nogo-A, or 7B12, directed against rat aa 763–820 of Nogo-A (Oertle *et al.*, 2003), or control monoclonal antibody against wheat auxin, were applied as highly purified IgGs at a concentration of 3 μg/mL in the culture medium for a period of 5 days (medium was changed every 2 days). For the regeneration studies, cultures underwent lesions (a mechanical transection at the level of CA3–CA1 junction), which were performed at room temperature with a sterile razor blade after 21 days *in vitro* (DIV). Antibody treatment was delivered immediately after transection.

The Nogo-A antibodies 11C7 and 7B12 were shown to enhance neurite outgrowth of neurons plated on Nogo-A-containing substrate *in vitro* (Oertle *et al.*, 2003) and in the injured CNS *in vivo* (Wiessner *et al.*, 2003; Liebscher *et al.*, 2005). They recognize Nogo-A specifically on Western blot (Oertle *et al.*, 2003; Dodd *et al.*, 2005).

Tissue collection was performed in accordance with the National Institutes of Health Guide for Care and Use of Laboratory Animals. All procedures have been approved by the Swiss Federal Veterinary Office.

Electrophysiology

Electrophysiological recordings were made using a multi-electrode array (MEA; Mielke *et al.*, 2005). Slices were cultured and recorded on sterilized and disposable cartridges that include a MEA consisting of 40 electrodes (30 μm thick) made of pure gold by plasma evaporation (Biocell Interface, SA, La Chaux-de-Fond, Switzerland). The MEA is built on a porous and transparent membrane that is maintained in a sandwich between two chambers: the upper chamber is the gas perfusion chamber that maintains the tissue at the gas–liquid interface; and the lower one is the perfusion chamber that contains sterile culture medium under perfusion. The chambers and the array are assembled and inserted into a console unit (Biocell Interface) where the temperature (33°C) and the perfusion parameters (10 μL/min) can be precisely monitored. The position of the slices on the electrodes can be visualized directly through the camera integrated within the connector. Each electrode can be assigned as stimulating or recording. Two recording sessions were usually performed: one before the lesion and a second at Day 6 post-lesion. In both sessions, four electrodes located in the CA1 area were selected for recording of synaptic responses evoked by two stimulating electrodes located in the CA3 area. This stimulation paradigm yielded the activity across the lesion. In addition, we also monitored activity in the mossy fibre connection, using two stimulating electrodes located in the dentate hilus and four recording electrodes located in the intact part of the CA3 area, close to the site of lesion. This stimulation paradigm was used to assess the viability of the tissue. Stimulation parameters were maintained constant in all sessions (pulses of 4 V, 0.5 ms, applied every 15 s). The amplitude of responses recorded during the 10-min period of both sessions (pre- and post-lesion) was averaged. The percentage of activity recorded at the second session was compared with that of the first session (assigned as 100% – pre-lesion). These percentages were then used for statistical analysis. Data are expressed as mean ± SEM of the number of slice cultures analysed, and statistical analyses were carried out using the unpaired *t*-test.

Immunofluorescence

Cultures were fixed with 4% paraformaldehyde overnight, after 5 DIV, 21 DIV, 21 DIV + 5 days treatment or 21 DIV + lesion + 5 days treatment, and then kept overnight in permeabilization buffer [1.5% horse serum, 3% Triton-X and 0.2% Top-Block (Juro AG, Lucerne, Switzerland), in phosphate-buffered saline 1x]. Primary antibody incubation with rabbit polyclonal anti-neurofilament 68 (NF68; AB1983, dilution 1 : 300; Chemicon International, Temecula, CA, USA), rabbit polyclonal anti-growth-associated protein 43 (Gap43; AB5220, dilution 1 : 1000; Chemicon International), mouse monoclonal anti-NeuN (MAB377, dilution 1 : 300; Chemicon International), mouse monoclonal anti-microtubule-associated protein 2a/b (MAP2a/b; ab3096, dilution 1 : 300; Abcam, Cambridge, UK), mouse monoclonal anti-CNPase (MAB326, dilution 1 : 1000; Chemicon International) or rabbit polyclonal anti-Nogo-A (Laura, produced in our laboratory; Oertle *et al.*, 2003) was performed in the permeabilization buffer for 5 days at 4°C. After washing, secondary antibody, Alexa 488 anti-mouse or Alexa 546 anti-rabbit (Invitrogen-Molecular Probes, Basel, Switzerland), was incubated for 2 h. Cultures were mounted on glass slides with Dako fluorescence mounting medium (Dako, Glostrup, Denmark).

For lower magnification imaging and densitometric analysis, cultures were imaged with a cooled CCD Camera CoolSNAP (Roper Scientific, Ottobrunn, Germany) coupled to a Zeiss Axioskop2 mot plus interfaced by MCID 7.0 Imaging System (Imaging Research, Ontario, Canada) with a 40× oil immersion objective (Plan NEOFLUAR, 1.3 numerical aperture). Confocal imaging was performed using a Zeiss LSM 410 confocal laser-scanning microscope using lasers pretuned to 543 nm (Alexa 546) and 488 nm (Alexa 488) with a 63× oil immersion objective (Plan APOCHROMAT Oil, 1.4 numerical aperture), or a Spectral Confocal Microscope TCS SP2 AOBS (Leica) using a 63× oil immersion objective (HCX PL APO Oil, 1.32 numerical aperture). Confocal image acquisition consisted of approximately 25 images of Z-dimension with a step size of 0.3 μm and image size of 0.21 μm/pixel (512 × 512). The pinhole was set at 1 Airy unit. Double-immunofluorescence staining was visualized with sequential acquisition of separate colour channels to avoid cross-talk between fluochromes. Maximum intensity projections of the images, using IMARIS software (Bitplane AG, Zurich, Switzerland), were used to improve the signal-to-noise ratio.

Quantification of axons and dendrites stained for NF68 or MAP2a/b

Organotypic hippocampal slices cultured for 21 DIV were incubated with anti-Nogo-A antibodies (11C7 and 7B21) or control IgG for further 5 days. After fixation and immunohistochemical treatment described above, confocal images were taken with CA3 *stratum pyramidale* centred in the picture frame, and partly containing *stratum*

oriens and *stratum radiatum* (about 1/3 of the picture frame for each *stratum*). For NF68 quantification, a rectangle of fixed area (115 × 84 μm) was placed in the area of the *stratum oriens* where most fibres were present. Using IMARIS software (Bitplane AG, Zurich, Switzerland), each fibre in the field was manually traced across the image stack. The software then calculated how many fibres were present, their individual length and total length calculated as the sum of the length of all individual fibres. Due to the complexity of tracing of MAP2a/b-positive fibres, a densitometric analysis was applied. Images were taken in the same regions described above and IMAGEJ software (http://rsb.info.nih.gov/ij) was used to determine the overall signal intensity. Optical density readings for MAP2a/b were corrected by subtraction of non-specific background density determined in the MAP2a/b expression-free non-immunoreactive fimbria of the same culture. All imaging, coding and tracing were performed blindly.

Gene expression microarray

Each condition [non-treated (NT), IgG-, 11C7- and 7B12-treated] was analysed in triplicate, performing three independent experiments per condition. Upon the end of the treatment and culturing time (26 DIV), groups of 24 cultures per experiment were pooled together. Total RNA was extracted using the RNeasy Lipid Tissue Mini Kit (Qiagen, Hilden, Germany) according to the manufacturer's protocol with the addition of an on-column DNaseI digestion step. The quantity and quality of the extracted RNA were determined using a NanoDrop ND 1000 (NanoDrop Technologies, ThermoFisher Scientific, MA, USA) and a Bioanalyzer 2100 (Agilent, CA, USA). Only RNA samples with an integrity index = 9.0 as established by Bioanalyzer data have been used.

The total RNA extracted was then reverse-transcribed into cDNA with One-Cycle cDNA Synthesis Kit (Affymetrix, Santa Clara, CA, USA). The double-stranded cDNA was purified with a Sample Clean-Up Module (Affymetrix). The purified double-stranded cDNA was *in vitro* transcribed in the presence of biotin-labelled nucleotides using an IVT Labeling Kit (Affymetrix). The biotinylated cRNA was purified using a Sample Clean-Up Module (Affymetrix), and its quality and quantity were assessed using a NanoDrop ND 1000 (NanoDrop Technologies, ThermoFisher Scientific) and a Bioanalyzer 2100 (Agilent). The biotinylated cRNA samples (10 μg) were fragmented randomly to 35–200 bp at 94°C in Fragmentation Buffer (Affymetrix), and were mixed in 300 μL of Hybridization Buffer containing a hybridization control cRNA and Control Oligo B2 (Affymetrix), 0.1 mg/mL herring sperm DNA and 0.5 mg/mL acetylated bovine serum albumin in 2-(4-morpholino)-ethane sulphonic acid (MES), pH 6.7 before hybridization to GeneChip® Rat Expression Array 230 2.0 (Affymetrix) for 16 h at 45°C. Arrays were then washed using a Affymetrix Fluidics Station 450 FS450_0001 protocol. An Affymetrix GeneChip® Scanner 3000 (Affymetrix) was used to measure the fluorescent intensity emitted by the labelled target.

Raw data processing was performed using the Affymetrix GCOS 1.4 software (Affymetrix). After hybridization and scanning, probe cell intensities were calculated and summarized for the respective probe sets by means of the MAS5 algorithm. To compare the expression values of the genes from chip to chip, global scaling was performed, which resulted in the normalization of the trimmed mean of each chip to target intensity (TGT value) of 500 as detailed in the statistical algorithms description document of Affymetrix (2002). Quality control measures were considered before performing the statistical analysis. These included adequate scaling factors (between 1 and 3 for all samples) and appropriate numbers of present calls calculated by application of a signed-rank call algorithm. The efficiency of the labelling reaction and the hybridization performance was controlled with the following parameters: present calls and optimal 3′/5′ hybridization ratios (about 1) for the housekeeping genes (GAPDH and ACO7), for the poly A spikein controls and the prokaryotic control (BIOB, BIOC, CREX, BIODN).

Further data analysis was performed by GeneSpring 7.2 (Silicon Genetics, Agilent, CA, USA). Values below 0.01 were set to 0.01. Each measurement was divided by the 50th percentile of all measurements in that sample. Each gene was divided by the median of its measurements in all samples. If the median of the raw values was below 10 then each measurement for that gene was divided by 10 if the numerator was above 10, otherwise the measurement was thrown out. A present call filter (two out of three present/marginal calls in at least one out of four different studied conditions) was applied. Data were statistically restricted through a one-way ANOVA ($P = 0.05$). A final threshold of = 1.2-fold increase or decrease in the expression level of each single transcript was applied. Regulated transcripts have been assigned to functional categories according to GeneOntology as well as literature and database mining (Pubmed http://www.ncbi.nlm.nih.gov/sites/entrez/; Bioinformatics Harvester EMBL Heidelberg http://harvester.embl.de/; Rat Genome Database http://rgd.mcw.edu). The performed microarray experiments are MIAME compliant and data are available online at the GEO database: http://www.ncbi.nlm.nih.gov/geo/query/acc.cgi?token=bnqpbycoucks wfs&acc=GSE12483.

Quantitative real-time-polymerase chain reaction (qRT-PCR)

Ten candidate transcript changes were selected for further validation (Table 1) by TaqMan qRT-PCR. Probe design and experiments have been outsourced to GenXpro GmbH (Frankfurt, Germany). New batches of cultures were made and treated in order to generate biological and experimental triplicates of the four experimental groups analysed in the microarray experiment. Upon the end of the treatment, groups of 24 cultures were pooled together and total RNA was extracted using the RNeasy Lipid Tissue Mini Kit (Qiagen, Hilden, Germany) according to the manufacturer's protocol with the addition of an on-column DNaseI digestion step. The quantity and quality of the extracted RNA were determined using a NanoDrop ND 1000

TABLE 1. Quantitative TaqMan real-time-PCR validation and comparison with Affymetrix microarray results

Gene name	NCBI identification	Gene chip fold change		qRT-PCR fold change	
		11C7 vs. NT	7B12 vs. NT	11C7 vs. NT	7B12 vs. NT
Arhgap21	XM_001074395	0.686	0.677	1.499	1.073
Cdc42	BC060535			0.3797	0.4913
Egr1	NM_012551	0.758	0.790*	1.039	0.8147*
IL1β	NM_031512	1.321*	9.510*	2.204*	2.008*
Iqgap3	XM_001068995	1.389*	1.865	1.759*	0.9563
Lgals9 (Galectin-9)	U72741	1.713	2.811	0.6058	1.109
Nrp1	NM_145098	0.788	0.594	3.3872	1.797
Rac2	BC086399	2.709*	4.414*	1.549*	1.396*
Slc6a12 (vGAT)	NM_017335	1.278*	3.505*	1.740*	1.170*
SLPI	NM_053372	10.61	45.60*	0.7982	1.493*
Timp1	NM_053819	1.885*	3.231*	6.510*	2.940*

*Microarray transcripts that were validated by qRT-PCR.

(NanoDrop Technologies, ThermoFisher Scientific) and a Bioanalyzer 2100 (Agilent). As for the microarray experiment, only RNA samples with an integrity index = 9.0 have been used. Probes were designed based on complete cDNA NCBI sequences (Table 1). All qRT-PCR experiments were performed by application of a OneStep-Taqman PCR with FAM-BBQ probe and ROX (passive reference). RNA (10 ng) was templated in each reaction of 20 μL. The OneStep RT-PCR Mastermix contained Hotstart Taq DNA polymerase, optimized reaction buffer, 5 mM (final concentration) $MgCl_2$, nucleotides (including dUTP) and reverse transcriptase combined with RNAse inhibitor. Generally, 45 cycles of amplification were used. To standardize the amount of sample added to a reaction, amplification of GAPDH as endogenous reference control was performed, running amplifications in separate tubes. Quantification was performed according to the Guide to Performing Relative Quantitation of Gene Expression Using Real-Time Quantitative PCR (Applied Biosystems, Foster City, CA, USA) using the comparative CT method.

Immunoblot analysis

Nogo-A antibodies specificity assay

Adult hippocampi from three Long–Evans rats and one Nogo-A knockout adult mouse were dissected and transferred to CHAPS lysis buffer [50 mM NaH_2PO_4 pH 8.0, 150 mM NaCl, 0.5% CHAPS, protease inhibitor cocktail (Roche, Basel, Switzerland)] on ice. Tissues were disrupted using a rotor-stator homogenizer. After 30 s on ice, samples were centrifuged (15 s, 2000 ***g***, 4°C) and total protein concentration of the supernatant was determined using a NanoDrop ND 1000 (NanoDrop Technologies, ThermoFisher Scientific, Wilmington, DE, USA). Samples (30 μg/lane) were resolved by 7–14% NuPAGE (Invitrogen, Carlsbad, USA) and transferred onto polyvinylidenedifluoride membranes. After blocking, incubation with 11C7 (1 : 15 000) and 7B12 (1 : 1000) primary antibodies at 4°C overnight followed. After washing membranes were incubated with horseradish peroxidase-conjugated secondary antibodies. Immunoreactive proteins were detected by a chemiluminescent substrate (SuperSignal West Pico, Pierce Biotechnology, Rockford, IL, USA). Images were captured with Stella system (Agilent Technologies).

Gap43 analysis of lesioned cultures

Six hippocampal cultures were pooled and lysed in buffer containing 1% Nonidet P-40, 1% sodium cholate, 0.05% sodium dodecyl sulphate (SDS), 20 mM Tris pH 7.5 and 100 mM NaCl, and then sonicated. Protein concentration was determined using the Bradford dye-binding assay (Bio-Rad, Hercules, CA, USA), according to the manufacturer's protocol, with bovine serum albumin as standard. Total protein (15 μg per lane) was separated by SDS–polyacrylamide gel electrophoresis (10%) under reducing conditions and blotted onto pure nitrocellulose membranes (Bio-Rad, Hercules, CA, USA). Membranes were incubated with antibodies against Gap43 (1 : 1000, polyclonal GAP-43; Chemicon) and β-actin (1 : 5000; Chemicon), followed by a horseradish peroxidase-conjugated secondary antibody (1 : 5000; Bio-Rad). The immunoreactive proteins were detected with an enhanced chemiluminescence kit (ECL; Amersham Pharmacia, Piscataway, NJ, USA) according to the manufacturer's protocol, by using ECL-Hyperfilm (Amersham Pharmacia, Buckinghamshire, UK). Quantification of signal intensities was performed using IMAGEJ software (http://rsb.info.nih.gov/ij). Densitometry values have been normalized to the IgG pooled cultures (IgG = 1.0).

Statistical analysis

Statistical analysis was performed using GRAPHPAD Prism software version 4 for Windows (La Jolla, CA, USA). A Mann–Whitney test was applied in all analyses, except for the electrophysiological data, where an unpaired *t*-test has been applied. Results are expressed in mean ± SEM.

Results

Nogo-A expression in young and differentiated organotypic hippocampal slice cultures

Hippocampal slices dissected from P7 rats are known to develop into mature, differentiated and functional circuits within 3 weeks (Gahwiler, 1981a,b,c; Stoppini *et al.*, 1991, 1993; Bahr, 1995; Noraberg *et al.*, 2005). A morphological analysis of the 21 DIV slice cultures using the neuronal nuclear marker NeuN (Mullen *et al.*, 1992; Lind *et al.*, 2005) showed that our cultures maintained the typical cytoarchitecture of the hippocampus, which is highly similar to its *in vivo* morphology (Fig. 1A and B).

In both young (5 DIV) and differentiated (21 DIV) cultures, Gap43 was expressed in CA3 neuronal processes (Fig. 2A and A′). NF68 expression changed from a high cell body expression in CA3 pyramidal cells in young cultures (Fig. 2B) to a low cell body expression and more expanded axonal expression in differentiated cultures (Fig. 2B′). While NF68 was expressed mainly in axons even if also present in dendrites, MAP2a/b was expressed only in dendrites (Fig. 2C, C′ and D, D′) throughout culture development.

In line with *in vivo* development (Berger & Frotscher, 1994), hippocampal slice cultures showed an increase in the expression of CNPase, an oligodendrocyte marker, as the cultures matured (Fig. 3A and A′). Nogo-A expression shifted from a primarily neuronal expression in young cultures (Fig. 3B and C) to a highly oligodendrocytic expression in the differentiated cultures (asterisk in Fig. 3B′), although pyramidal cells still expressed Nogo-A (Fig. 3B′ and C′). This effect was gradual, however, as some oligodendrocytes expressing Nogo-A could already be observed in the young cultures (arrow in Fig. 3C), and lower level of Nogo-A expression persisted in pyramidal neurons of the CA3 region in the differentiated cultures (Fig. 3C′), similar to the adult *in vivo* situation (Trifunovski *et al.*, 2006). During the development of the cultures, it was always possible to detect cells positive for both CNPase and Nogo-A, although at early time points not all CNPase-positive cells were also Nogo-A positive (Fig. 3D and D′). The increased co-labelling of CNPase and Nogo-A with slice culture maturation is in line with the observed increase of Nogo-A expression in oligodendrocytes.

Nogo-A neutralization enhances regeneration of transected Schaffer collaterals

A sharp cut through the border between the regions CA3 and CA1 of 21 DIV organotypic hippocampal slice cultures was made with a sterile razor blade. The cultures were incubated with the Nogo-A-specific neutralizing antibody 11C7 (Fig. 1C), with control antibodies or with culture medium alone for an additional 5 days. Field potentials were evoked by stimulation of the CA3 region and recorded in CA1 before (21 DIV) and 5 days after lesion and antibody treatment (26 DIV). The organotypic hippocampal slices were cultured on MEAs for 21 days (Fig. 4A). The lesion was complete as no activity could be elicited across the lesion site immediately after the cut; additionally the trace of the razor blade is visible in the MEA culture

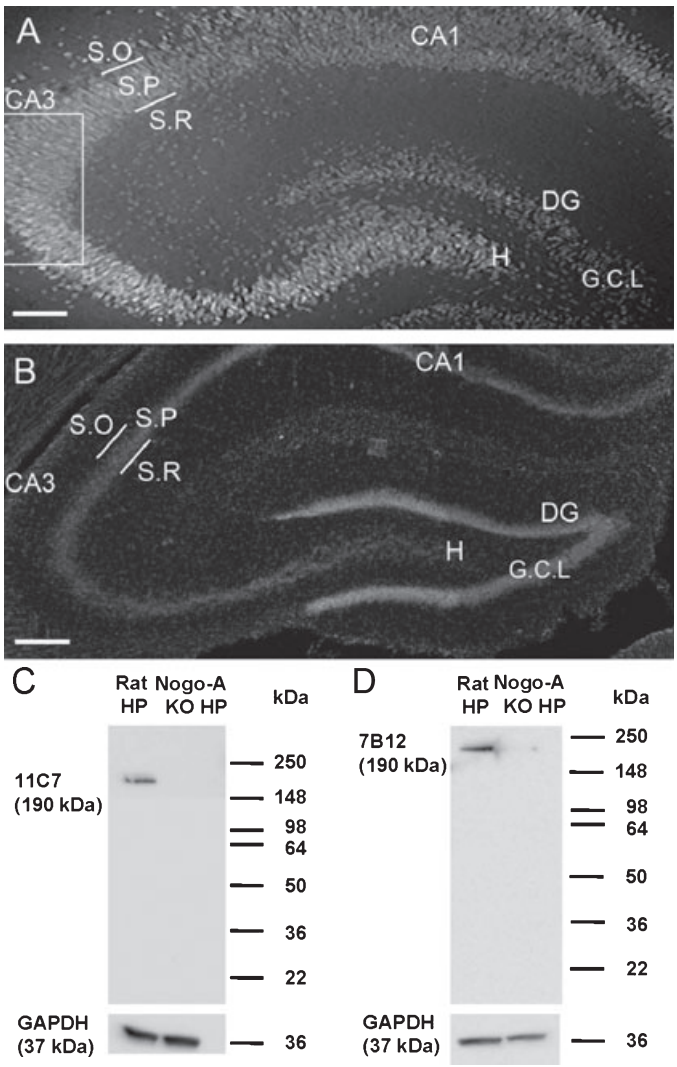

FIG. 1. Hippocampal organotypic slice culture morphology and antibody specificity. (A) Typical architecture of pyramidal and granular cell layers in organotypic hippocampal cultures after 3 weeks *in vitro*. The box depicts the region where all subsequent imaging and analysis took place. (B) Adult hippocampus *in vivo* (adult rat). Both *in vitro* culture and *in vivo* section are labelled with NeuN. (C and D) Images of immunoblots showing the specificity of the anti-Nogo-A antibodies for 11C7 (C) and 7B12 (D). Note the single band detected with the total protein extract of the rat hippocampus, which is not detected with the total extract of hippocampus of Nogo-A knockout mice. Scale bars: 140 μm (A); 260 μm (B). DG, dentate gyrus; G.C.L, granular cell layer; H, hilus; S.O, stratum oriens; S.P, stratum pyramidale; S.R, stratum radiatum.

shown in Fig. 4A. When the CA3 region was stimulated 5 days after lesion, the amplitude of the evoked potentials recorded in CA1 was 68.32 ± 4.583% SEM of the recorded values in intact slices for the 11C7 anti-Nogo-A antibody-treated group, while the injured control antibody-treated group showed only an average evoked potential amplitude of 37.25 ± 3.443% SEM of that of the intact tissue (Fig. 4D; $P = 0.0005$, Mann–Whitney).

The averaged trace representation of the evoked potentials showed the increased amplitude of the response after Nogo-A neutralization (Fig. 4F), while the control IgG-treated cultures showed much lower evoked potentials (Fig. 4E). An additional control for neuronal viability was the stimulation of CA3 and recording of CA3 potentials (Fig. 4C), which showed no difference across the groups, therefore indicating that the effect observed with anti-Nogo-A antibody treatment was not due to improved neuronal survival but rather to enhanced restoration of the connection of CA3 to CA1, i.e. the injured Schaffer collaterals. Not a single culture with evidence of epileptic activity was observed, neither in the control nor in the anti-Nogo-A antibody-treated groups. The improvement in evoked potential responses seemed to be due to the increased number of fibres that grew across the lesion site. Immunofluorescence detection of the important axonal growth marker Gap43 on the lesioned cultures revealed an increased number of fibres crossing the lesion site after Nogo-A neutralization (arrows in Fig. 4G and H) when compared with the control IgG treatment (arrows in Fig. 4F). After Nogo-A neutralization, it was even possible to detect growth cone-like structures (arrowhead in Fig. 4H). Within the 5 days of treatment after the lesion, Gap43 levels increased 1.28-fold in the lesioned anti-Nogo-A antibody-treated cultures as compared with the lesioned control IgG-treated ones (Fig. 4I). On the other hand, the rise in Gap43 expression levels after Nogo-A neutralization in the control unlesioned cultures was not striking. Our results show that suppression of Nogo-A for 5 days in the lesioned adult hippocampus enhanced functional regeneration of the CA3–CA1 Schaffer collaterals, reflected at the molecular level by the upregulation of Gap43 and histologically by Gap43-positive fibres that crossed the lesion site, in the absence of aberrant growth in the dentate gyrus and CA3 that would lead to epileptic activity.

Nogo-A neutralization potentiates the axonal growth machinery in intact differentiated slice cultures

The regeneration results laid the ground for the question of axon growth in response to Nogo-A neutralization in 21 DIV intact cultures as a model of the intact hippocampus. After 5 days of treatment (26 DIV) with either one of two function-blocking-specific anti-Nogo-A antibodies, 11C7 or 7B12 (Fig. 1C), we observed a significant increase in the number of fibres labelled for NF68 [Figs 5(C and D) and 6A] when compared with control antibody treatment or untreated cultures in the CA3 region [Figs 5(A and B) and 6A]. Additionally, there was a significant increase in the total fibre length of the cultures treated with the two anti-Nogo-A antibodies (Fig. 6B), reflecting the increased number of fibres detected as no significant differences between the different treatment groups in terms of mean, maximum or minimum fibre length (data not shown) were present. Mean maximum, minimum and length of fibres were approximately 105, 3.3 and 28 μm, respectively. In contrast to NF68, MAP2a/b did not show detectable differences across the four different treatment groups [Figs 5(A′–D′) and 6C]. NF68 is mainly expressed in axons, while MAP2a/b is a dendritic marker (Fig. 2D and D′), thus due to the lack of an increase in MAP2a/b immunostaining we suggest that the observed increase in NF68-positive fibres in the anti-Nogo-A-treated cultures might most likely be due to axonal longitudinal or axial growth, sprouting and arborization.

Though potentially expected, stimulation/recording experiments showed that there were no detectable changes in the evoked activity of the unlesioned antibody-treated cultures (Fig. 6D) and, most importantly, as previously shown for lesioned cultures (see above), no evidence of epileptic activity could be observed, neither in control IgG-treated nor in anti-Nogo-A-treated intact cultures.

Gene expression changes induced by Nogo-A neutralization

In order to better understand the mechanisms by which Nogo-A neutralization induces the above-mentioned morphological changes, a

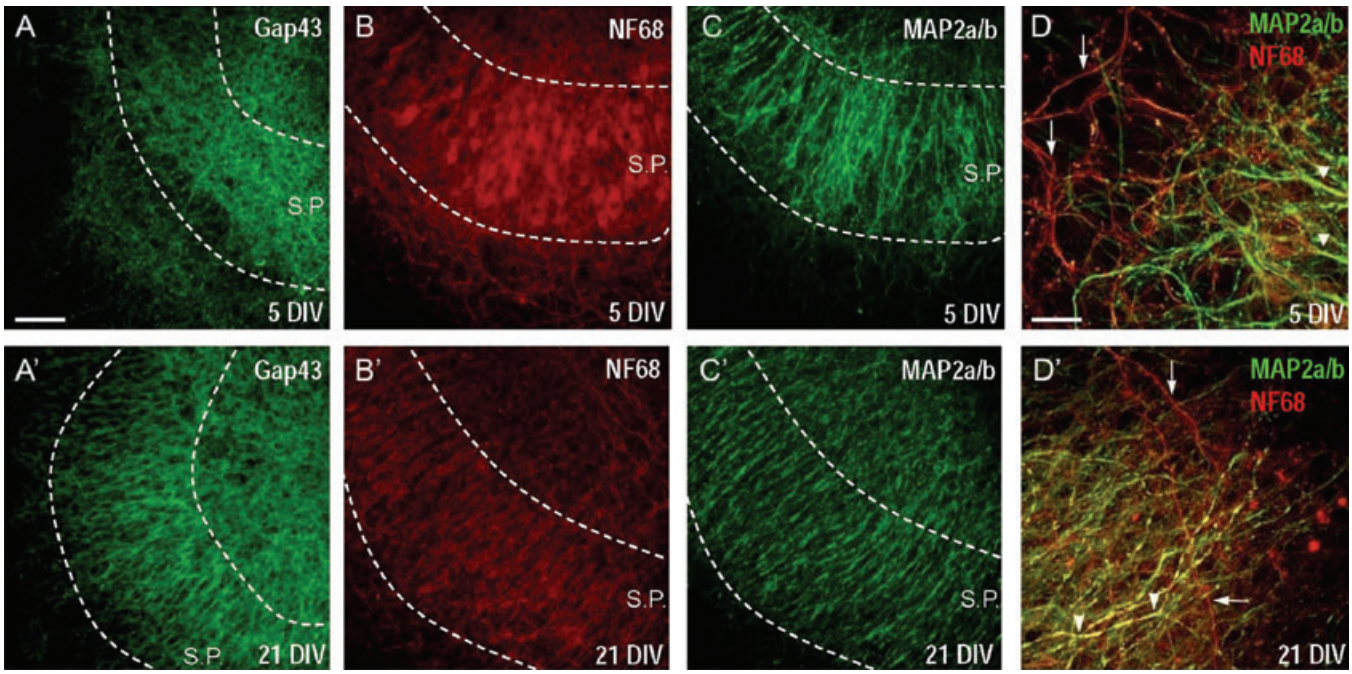

FIG. 2. Neuronal marker expression in young (5 DIV: A–D) and differentiated cultures (21 DIV: A′–D′). CA3 pyramidal neurons in the stratum pyramidale (S.P.) and their axons are positive for Gap43 (A, A′), NF68 (B, B′), and their dendrites, mainly in stratum pyramidale, are positive for MAP2a/b (C, C′) in young cultures (A–D) and differentiated cultures (A′–D′). Note predominant cell body labelling of NF68 in young cultures (B). Dashed lines represent the borders of stratum pyramidale. (D, D′) Overlay from (B and C), showing in red NF68 axonal labelling (arrows in D, D′) and dendritic co-labelling of NF68 (red) and MAP2a/b (green) in yellow (arrowheads in D, D′) on both young and differentiated cultures. Scale bars: 100 μm (A–C and A′–C′); 40 μm (D and D′).

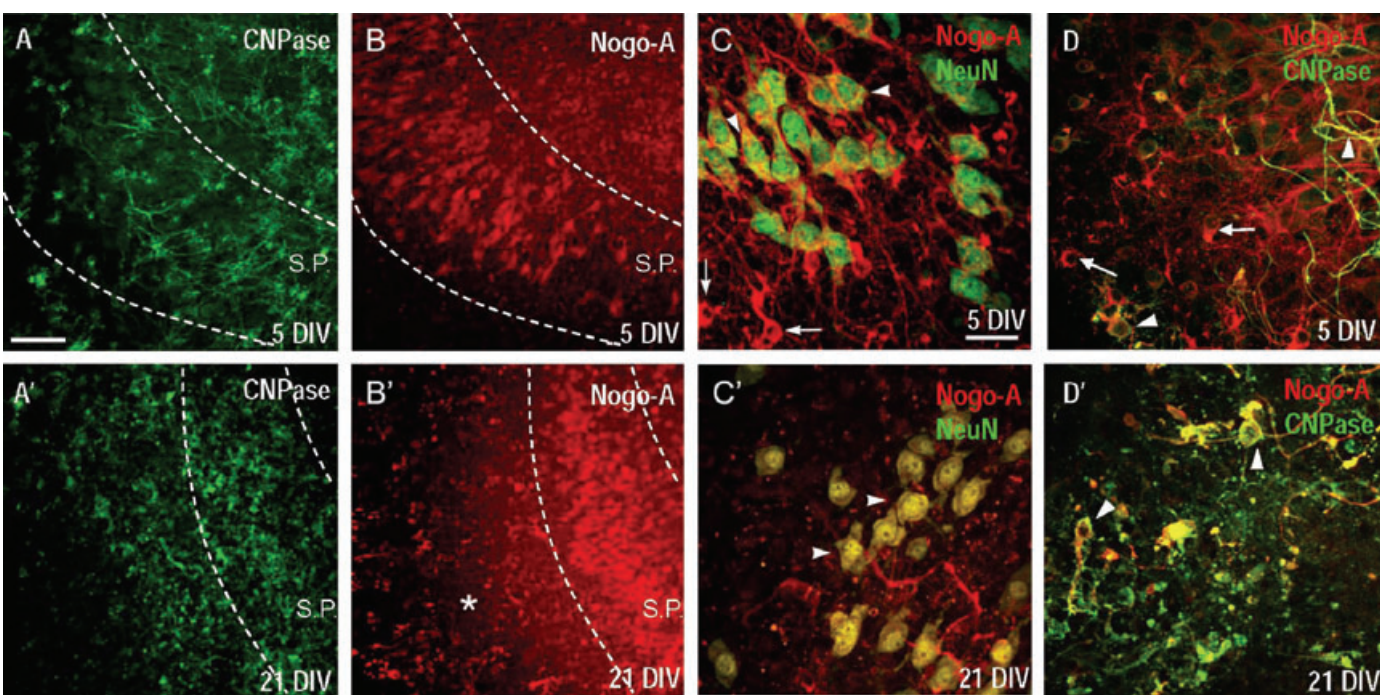

FIG. 3. Oligodendrocyte marker and Nogo-A expression in young (5 DIV: A–D) and established cultures (21 DIV: A′–D′). Oligodendrocytes labelled for CNPase are present in greater amounts in established (21 DIV) cultures (A′) compared with young (5 DIV) cultures (A). Co-labelling between Nogo-A and CNPase is almost complete in 21 DIV cultures, while in 5 DIV cultures some CNPase cells do not express detectable levels of Nogo-A. Nogo-A is most prominently expressed in pyramidal neurons (B, arrowheads in C) of young cultures. Some Nogo-A-positive oligodendrocytes are present in young cultures (arrows in C; NeuN in green). In differentiated cultures Nogo-A is most prominently expressed in oligodendrocytes (asterisk in B′), but is still present in pyramidal cells (arrowheads in C′; NeuN in green). Young cultures show cells that are Nogo-A-positive but CNPase-negative (arrows in D), and others which are Nogo-A- and CNPase-positive (arrowheads in D). In mature cultures, on the other hand, almost all CNPase-positive cells are also Nogo-A-positive (arrowheads in D′), confirming the described localization on Nogo-A in oligodendrocytes. Dashed lines represent the borders of stratum pyramidale. Scale bars: 100 μm (A, B and A′, B′); 40 μm (C, D and C′, D′).

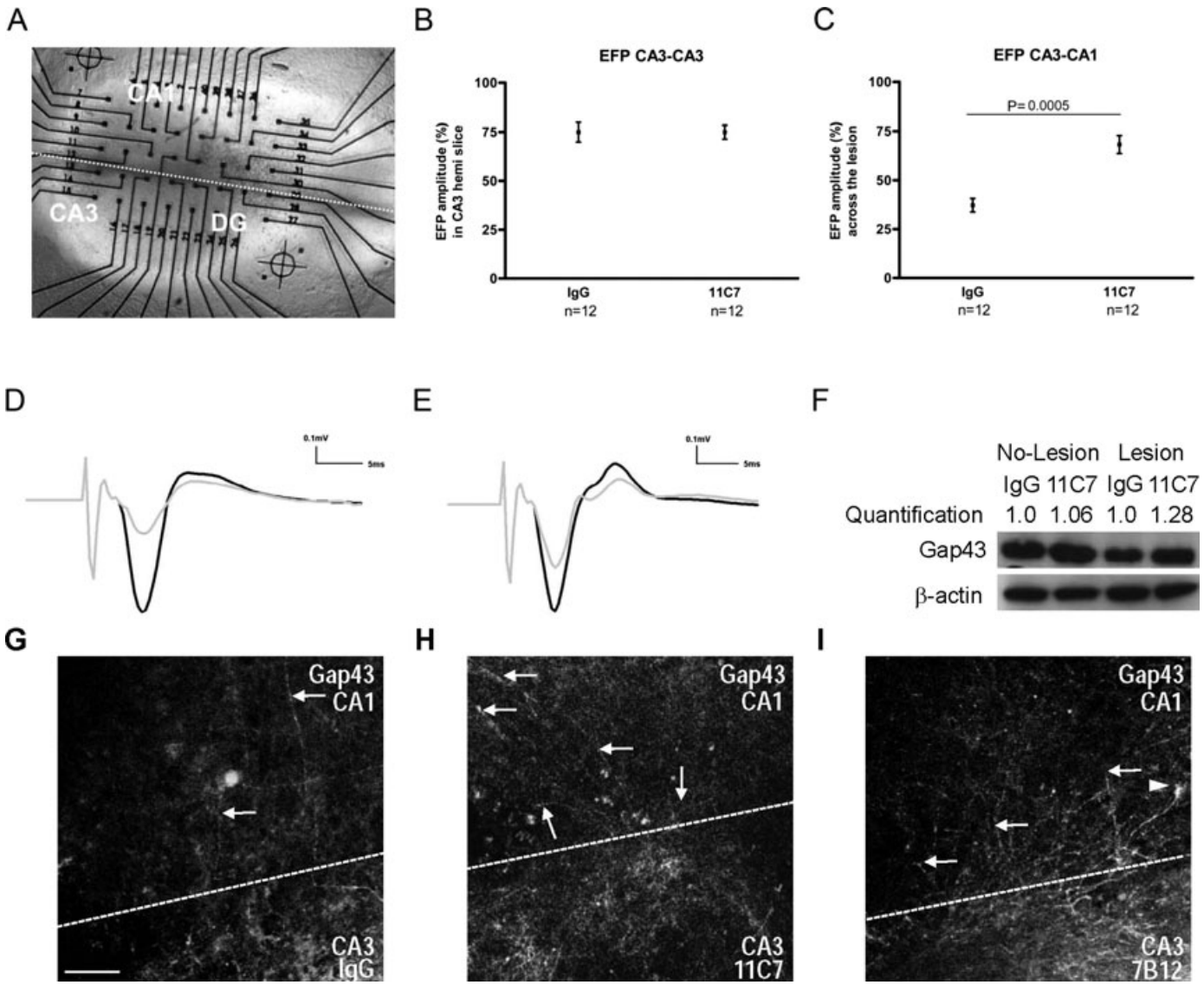

FIG. 4. Effect of Nogo-A neutralization on Schaffer collateral regeneration of 21 DIV organotypic hippocampal slice cultures. Organotypic hippocampal slice cultures were cultured for 21 days. The Schaffer collaterals were cut and function-blocking antibodies against Nogo-A were added to the culture medium for an additional 5 days. (A) Micrograph of an organotypic hippocampal slice culture grown on the MEA. Dotted line indicates the razorblade lesion. (B) No change in the mean amplitude of evoked field potentials in control CA3 stimulation–CA3 recording after lesion and 5-day treatment with control IgGs (IgG) or anti-Nogo-A antibody (11C7). n = 12 slice cultures. (C) Increased evoked responses in CA1 after CA3 stimulation in injured, anti-Nogo-A antibody (11C7)-treated cultures as compared with control antibody treatment (IgG). 11C7 = 68.32 ± 4.583% SEM; IgG = 37.25 ± 3.443% SEM; n = 12 slice cultures; P = 0.0005, Mann–Whitney test. Averaged traces of the evoked potentials of control IgG (D) and anti-Nogo-A-treated slice cultures (E), before (black lines) and after lesion and treatment (grey lines). (F) Gap43 Western blot from six pooled cultures treated with IgG control or 11C7, showed a 1.28-fold increase in Gap43 content after lesion and subsequent treatment with 11C7 as compared with subsequent control IgG treatment. The cultures with no lesion had a minimal Gap43 increase after Nogo-A neutralization. β-Actin was used as loading control and the intensities of the bands were used to normalize Gap43 intensities in the corresponding treatments. (G–I) Gap43 fibres crossing the lesion site (dotted line) from CA3 to CA1 areas. Few fibres (arrows) were detected with the control IgG treatment (G), while more fibres were detected with the neutralization of Nogo-A with 11C7 (H) or 7B12 (I). Note the growth cone-like structure (arrowhead in I) that is visible in the CA1 region past the lesion site. Scale bar: 40 μm (G and H).

transcriptomic analysis was performed. Total RNA was extracted from 26 DIV slice cultures NT, or treated from Days 21 to 26 with anti-Nogo-A antibodies (11C7 or 7B12), or with control antibodies (IgG). We compared 11C7 vs. NT, 7B12 vs. NT and IgG vs. NT conditions, and generated lists of transcripts up- or downregulated = 1.2-fold. Transcripts commonly regulated in 11C7 (11C7 vs. NT) and 7B12 (7B12 vs. NT) treatment, and excluding those that were shown as being regulated also by the control IgG treatment (IgG vs. NT) itself, have been considered of particular interest (Fig. 7; Table 2). Ninety-five genes were differentially expressed at 26 DIV after 5 days of Nogo-A neutralization and common to both anti-Nogo-A antibody treatments (11C7 and 7B12). When assigned to functional categories (Fig. 7; Table 2), 29.9% of the listed transcripts could be placed under a major category of growth-related genes comprising cell adhesion, extracellular matrix (ECM), growth factor, GTPase signal transduction, neurogenesis and neuronal survival. Interestingly, the third largest category – 8% of regulated transcripts – was GTPase signal transduction and GTPases regulators. This cluster includes molecules

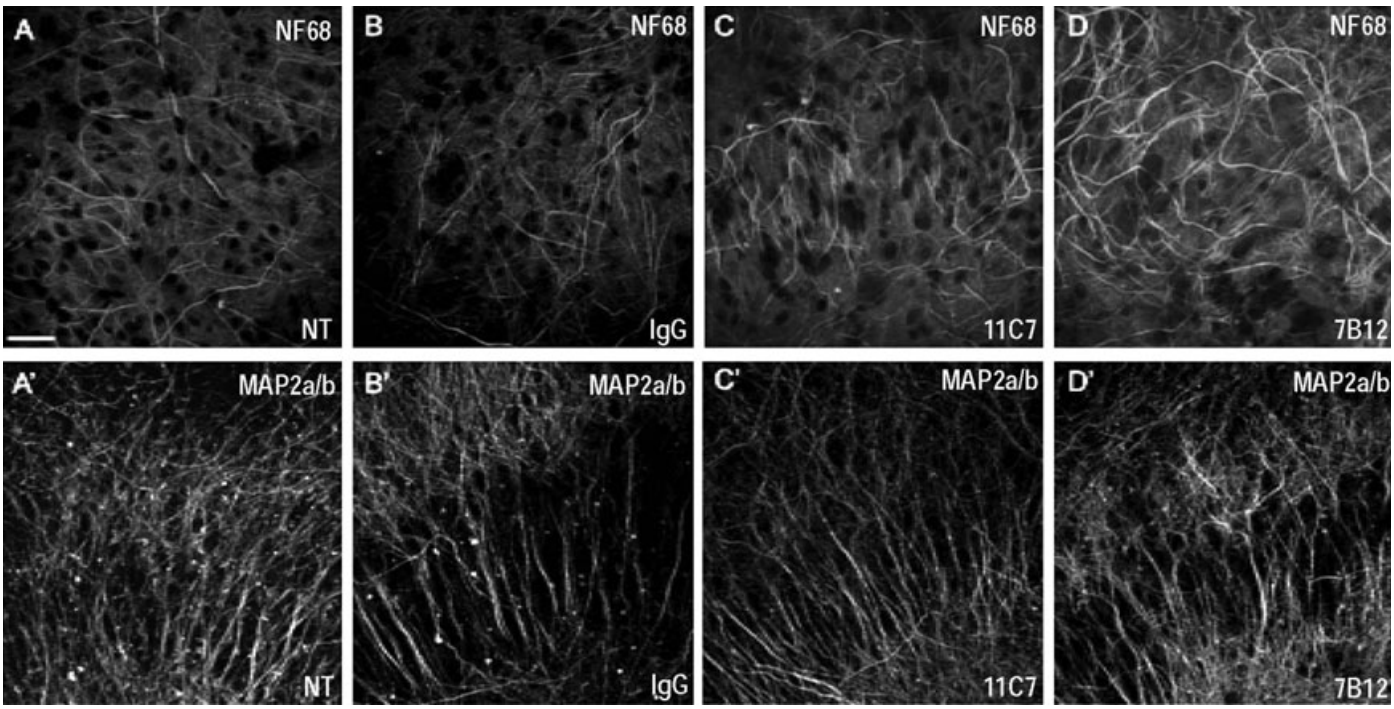

FIG. 5. Effect of Nogo-A neutralization in 21 DIV non-injured organotypic hippocampal cultures. Organotypic hippocampal cultures were cultured for 21 days and subsequently received a 5-day treatment with medium alone (A, A′), control IgG (B, B′), or with anti-Nogo-A antibodies 11C7 (C, C′) and 7B12 (D, D′). An increase in the number of fibres positive for NF68 in CA3 region after anti-Nogo-A antibody incubation 11C7 (C) and 7B12 (D) compared with medium alone NT (A) or control IgG treatment (B) indicates an increase of the growth properties of CA3 hippocampal neurons. MAP2a/b fibre density remained similar across treatments, medium alone NT (A′), IgG control (B′), 11C7 (C′) and 7B12 (D′) indicating the dendritic arborization was not detectably influenced by Nogo-A neutralization. Scale bar: 40 μm.

that belong to the family of small Rho GTPases, known to be crucially involved in Nogo-A signalling. In particular, RhoA and ROCK have been shown to be downstream effectors of the Nogo-A signalling pathway (Niederost *et al.*, 2002; Fournier *et al.*, 2003; Schweigreiter *et al.*, 2004; Hsieh *et al.*, 2006; McKerracher & Higuchi, 2006). We observe a regulation of: Rac2 (11C7 = 2.709; 7B12 = 4.414), Rho GTPase-activating protein 21 (Arhgap21; 11C7 = 0.686; 7B12 = 0.677) and IQ motif containing GTPase-activating protein 3 (Iqgap3; 11C7 = 1.389; 7B12 = 1.865). Among the growth factors and axonal growth-promoting transcripts, interleukin 1 beta (IL1β; 11C7 = 1.321; 7B12 = 9.510), transforming growth factor beta-regulated gene 1 (tbrg1; 11C7 = 1.249; 7B12 = 1.239), tissue inhibitor of metalloproteinase-1 (TIMP-1; 11C7 = 1.885; 7B12 = 3.231) were upregulated following Nogo-A neutralization, contrary to insulin-like growth factor 1 (Igf1; 11C7 = 0.654; 7B12 = 0.331), which was found to be downregulated. The second most upregulated gene after Nogo-A neutralization was secretory leukocyte protease inhibitor (SLPI; 11C7 = 10.61; 7B12 = 45.60), which is involved in immune processes and has been shown to play a role in neuroprotection.

Tables S1 and S2 in the supporting information list the regulated transcripts subdivided into functional categories that are unique to each one of the two anti-Nogo-A antibodies, 11C7 and 7B12. The main categories represented in Table 2 are also represented in supporting Tables S1 and S2. The same functional categories were generally regulated in the same direction, up- or downregulation by both treatments. Interestingly, 7B12 induced the regulation of a greater number of transcripts per category, with usually higher fold changes, when compared with 11C7. No gene expression change unique to IgG treatment could be placed into a growth-related category (Table S5). Many of the transcripts that were commonly regulated by all three treatments 11C7, 7B12 and IgG vs. NT showed opposite direction of regulation, up- or downregulation, if responding to the Nogo-A-specific antibodies or to the control IgG (Table S6). Such transcripts include the Slc6a12 from the neurotransmission category, and a vesicular γ-aminobutyric acid (GABA) transporter, which was upregulated after Nogo-A neutralization but downregulated after control IgG treatment. In those few cases in which the direction of expression change was the same, usually the IgG treatment caused lower fold changes, i.e. similar to CD2 antigen family member 10 (Slamf9) assigned to the ECM functional category (11C7 = 4.37; 7B12 = 9.72; IgG = 1.243). Only a few transcripts with regulations common to 11C7 and IgG treatment were in the same direction and similar in fold change levels (Table S3), suggesting that an unspecific effect of IgG type antibody treatment may be present. While more differences existed between genes commonly regulated by 7B12 and IgG treatment (Table S4), they were not related to growth responses, with the exception of distal-less homeobox 5 (Dlx5), a transcription factor involved in the development of the nervous system that was downregulated after Nogo-A neutralization but upregulated after IgG control treatment. Therefore we suggest that most of these differences could be due to unspecific effects of the IgG treatment.

A subset of 10 interesting transcripts regulated following 11C7 and 7B12 treatment have been further validated by qRT-PCR: Arhgap21, Egr1, IL1β, Iqgap3, Lgals9 (Galectin-9), Nrp1, Rac2, Slc6a12, SLPI, TIMP-1. We additionally tested for the potential regulation of Cdc42, not detected in the microarray approach but known to be regulated by Arhgap21 and Idgqp3 (see Discussion). Although the absolute values for the fold changes differ between the two techniques, the general direction of change was the same in 50% of the analysed transcripts for 11C7-induced changes and in 60% of the analysed transcripts for 7B12-induced changes (see Discussion). Changes in the transcripts

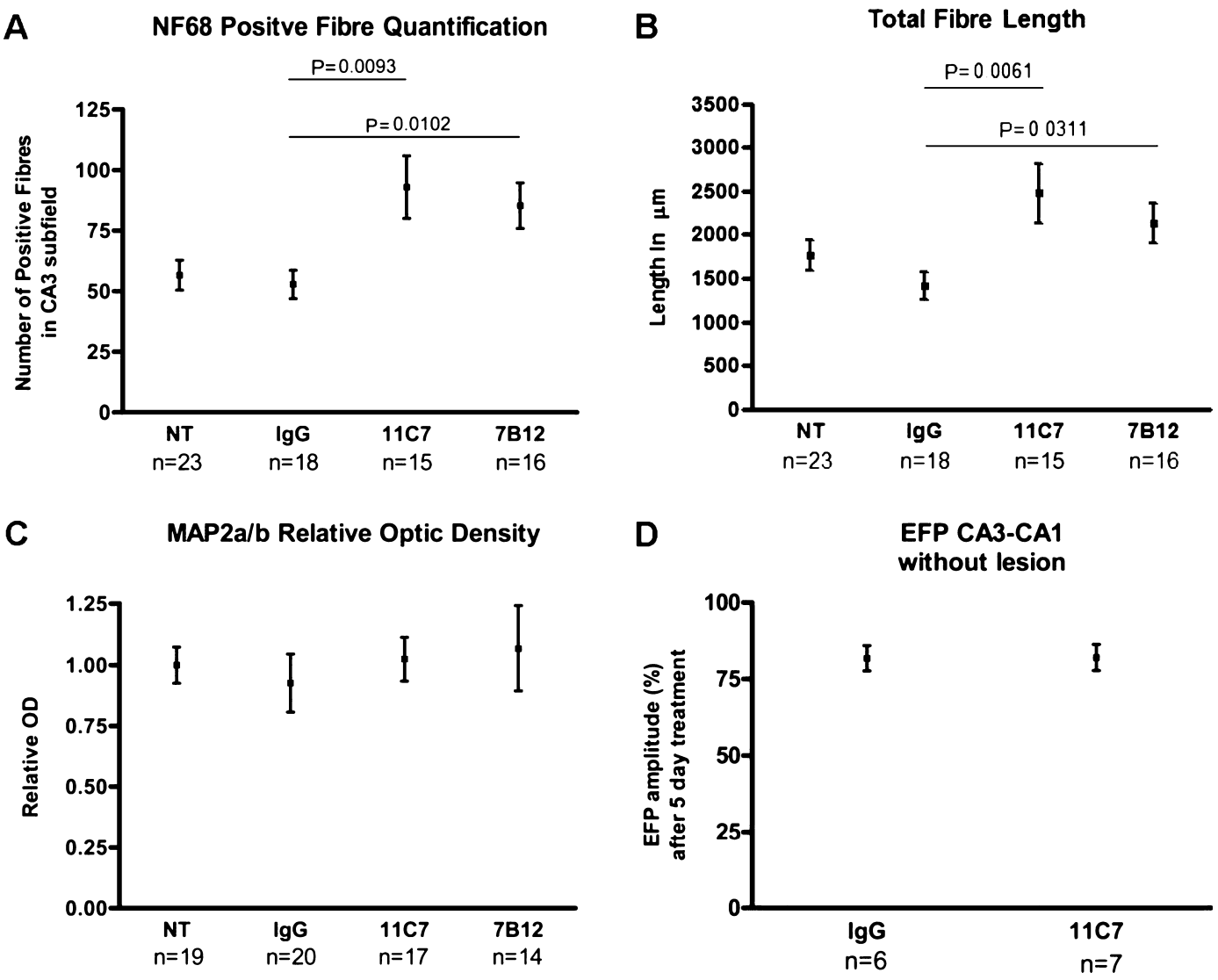

FIG. 6. Quantification of effect of Nogo-A neutralization in 21 DIV non-injured organotypic cultures. (A) Quantification of the number of NF68-positive fibres in the stratum oriens of CA3 area shown in Fig. 5 showed a significant increase in the number of fibres present after Nogo-A neutralization as compared with the control treatments. (B) Quantification of the total length of the NF68-positive fibres calculated has the sum of all individual fibres. (C) Densitometric analysis of MAP2a/b immunoreactivity in CA3 region revealed no differences between the different treatment groups. (D) Stimulation-induced activity in 21 DIV non-lesioned cultures grown on MEAs after a 5-day antibody treatment did not detect differences in the CA3–CA1-evoked potentials between the anti-Nogo-A and the control IgG-treated groups.

level for IL1β, Rac2, Slc6a12 and TIMP-1 were validated for both treatments (Table 1; Fig. 8).

Discussion

Using organotypic hippocampal slice cultures as a model, we show *in vitro* that neutralization of Nogo-A with specific function-blocking antibodies enhances sprouting, axonal regeneration and reconnection following a lesion. Interestingly, growth induction by antibody-mediated Nogo-A neutralization also occurred in intact differentiated cultures. mRNA profiling supported on a molecular level the morphological observation of a growth enhancement effect of Nogo-A neutralization and suggested the possible involvement of small Rho GTPases in Nogo-A as an underlying regulated signalling pathway. Therefore, Nogo-A seems to tonically suppress the growth machinery of pyramidal neurons in both lesioned and intact differentiated hippocampal tissue.

Organotypic hippocampal slice culture characterization

Organotypic slice cultures have been used frequently to study many aspects of brain function, development and regeneration (Gahwiler, 1981a,b,c; Stoppini *et al.*, 1991, 1993; Bahr, 1995; Mingorance *et al.*, 2006; Hakkoum *et al.*, 2007). We characterized our culture system by determining the expression of several markers. Using the oligodendrocyte marker CNPase, we observed an increase in the number of oligodendrocytes from cultures of 5 DIV to cultures of 21 DIV, indicating a maturation of these glial cells resembling the *in vivo* situation, as previously described (Berger & Frotscher, 1994). With the progression of culture maturation, the large majority of

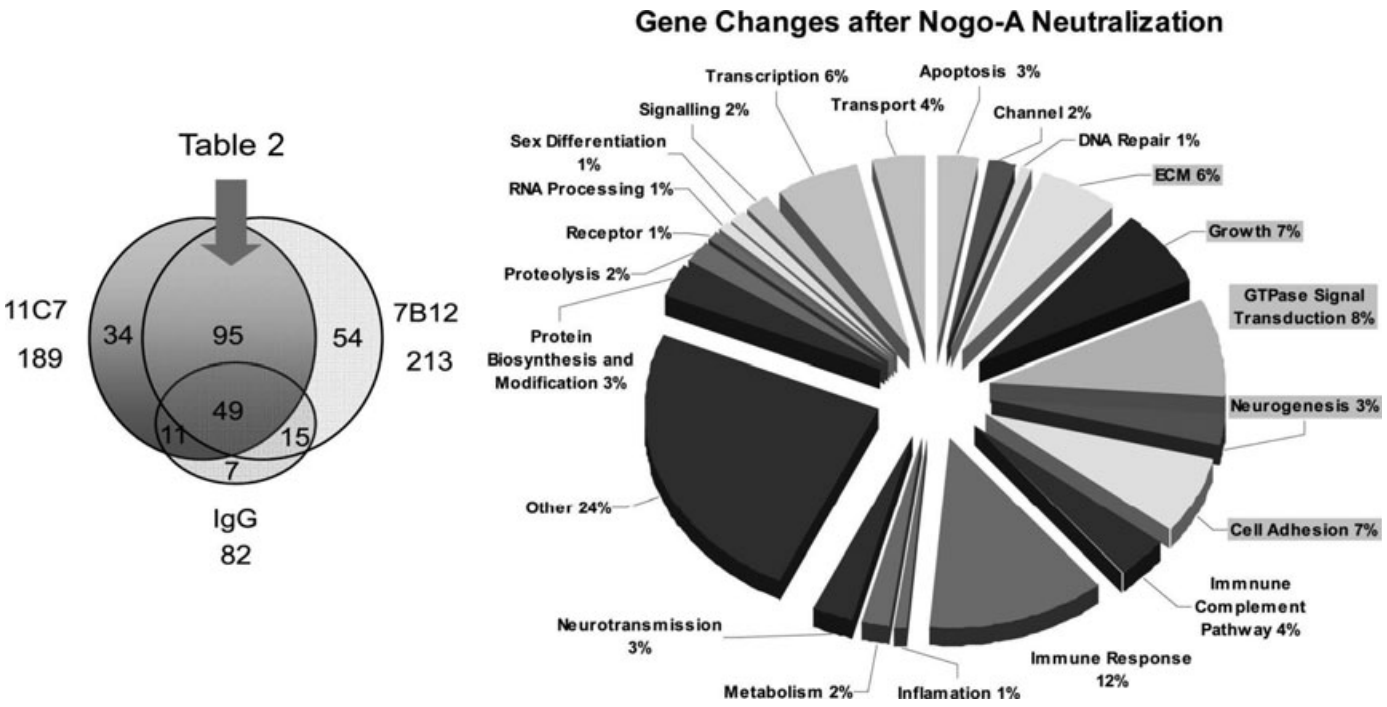

FIG. 7. Gene expression changes induced by Nogo-A neutralization, category assignment and gene proportions. Scheme depicting the gene distribution in the different treatment groups analysed and schematic representation of the proportion of genes specifically regulated after anti-Nogo-A treatment in different functional categories. Highlighted in grey boxes are the categories containing genes with influence in growth responses.

CNPase-positive oligodendrocytes also expressed Nogo-A, confirming the classical localization of Nogo-A in oligodendrocytes in mature CNS tissue.

In line with previous characterizations (Mielke *et al.*, 2005), the neuronal growth marker Gap43 remained expressed after 3 weeks in our cultures. The presence of NF68, a neurofilament protein localized in axons and dendrites (Shaw *et al.*, 1985; Kleiman *et al.*, 1990), was slightly increased during the maturation of the cultures. This was expected considering that NF68 is a core part of the developing and mature neurofilament cytoskeleton (Shaw & Weber, 1981; Reines *et al.*, 2004), and that during culture maturation new axons and connections are formed.

Nogo-A mRNA in the adult hippocampus has been shown to be localized both in neuronal cells and oligodendrocytes (Huber *et al.*, 2002; Meier *et al.*, 2003; Gil *et al.*, 2006; Trifunovski *et al.*, 2006). Our immunohistochemical study confirmed this localization at the protein level: Nogo-A protein was highly expressed in neuronal cells in the early stages of culturing, followed by oligodendrocyte expression and a decline to slightly lower amounts in the cell bodies of pyramidal cells.

Enhanced regenerative response after Nogo-A neutralization

Several groups have used organotypic hippocampal cultures as models to study regeneration after different types of lesions (Stoppini *et al.*, 1993, 1997; McKinney *et al.*, 1997, 1999; Mingorance *et al.*, 2006; Hakkoum *et al.*, 2007). Lesions separating CA3 from CA1 can lead to regeneration of Schaffer collaterals across the lesion site (McKinney *et al.*, 1997). In our control lesioned cultures, stimulation of CA3 lead to responses in CA1 at the level of approximately 35% of intact CA1 evoked field potential amplitude. Nogo-A neutralization for a 5-day period (21–26 DIV) following lesion induced a significant increase to approximately 65% of the response prior to injury, indicating functional regeneration and synaptogenesis. Accordingly, immunoblot and immunohistochemical analysis of the cultured tissue following Nogo-A neutralization showed an increase in the overall Gap43 level and in the number of Gap43-positive fibres growing across the lesion site. These results clearly demonstrate that Nogo-A neutralization enhanced the regenerative response.

Reactive sprouting after Schaffer collateral lesion can induce increased excitability ultimately leading to epileptic activity (McKinney *et al.*, 1997). We therefore tested for this parameter. In the present study, neither the recording of normal activity nor stimulation of CA3 with recording in CA3 or CA1 gave any indication of epileptiform activity in the lesioned organotypic hippocampal cultures following anti-Nogo-A treatment. We speculate that the absence of hyperexcitability in cultures treated with anti-Nogo-A antibodies might be related to an enhanced GABAergic activity as reflected by the increase in mRNA levels for the vesicular GABA transporter (11C7 = 1.278; 7B12 = 3.505; IgG = 0.795) observed in the intact cultures (Table S6).

Fibre growth induced in normal CNS tissue

We show an increase in the number and total length of fibres positive for NF68 after Nogo-A neutralization in differentiated 21 DIV organotypic hippocampal slices treated with antibodies for 5 days, indicating axonal growth/sprouting of uninjured fibres. These results are in line with previous reports of upregulation of genes related to axonal growth (Zagrebelsky *et al.*, 1998) and morphological evidence of sprouting in adult cerebellar Purkinje cells (Buffo *et al.*, 2000; Gianola *et al.*, 2003) after injection of three different anti-Nogo-A antibodies. In these previous experiments, the sprouting response was transient as about 1 month after the antibody interventions the aberrant sprouts disappeared. Similar results were obtained in the spinal cord's corticospinal tract fibres (Bareyre *et al.*, 2002). The higher number of

TABLE 2. Gene expression changes induced by Nogo-A neutralization

Gene symbol	Gene name	Accession number	11C7 Fold change	11C7 *P*-value	7B12 Fold change	7B12 *P*-value
Apoptosis (3%)						
Cipar1	Castration-induced prostatic apoptosis-related protein 1	1370962_at	1.627	0.0348	2.028	0.0348
Casp4	Caspase 4	1387818_at	1.403	0.0156	1.575	0.0156
Lcn2	Lipocalin 2	1387011_at	4.568	0.0361	11.5	0.0361
Cell adhesion (7%)						
Asgr1	Asialoglycoprotein receptor 1	1370149_at	1.522	0.038	5.801	0.038
Lgals5	Lectin galactose-binding soluble 5 (Galectin-5)	1369716_s_at	1.623	0.00838	2.381	0.00838
Alcam	Activated leukocyte cell adhesion molecule	1370043_at	0.812	0.0324	0.702	0.0324
Stab1_predicted	Similar to stabilin-1	1374247_at	1.587	0.00949	2.501	0.00949
Ncam2	Neural cell adhesion molecule 2	1384734_at	1.236	0.0499	0.729	0.0499
Lgals9	Lectin galactose-binding soluble 9 (Galectin-9)	1387027_a_at	1.713	0.0151	2.811	0.0151
Chi3l1	Chitinase 3-like 1 (cartilage glycoprotein-39)	1392171_a	1.314	0.0111	1.723	0.0111
Channel (2%)						
Cybb	Endothelial type gp91-phox gene	1373932_at	1.772	0.0231	3.712	0.0231
Cybb	Endothelial type gp91-phox gene	1379344_at	2.045	0.0129	3.65	0.0129
DNA repair (1%)						
Rad52_predicted	Rad52 protein	1377902_a_at	0.754	0.0414	0.739	0.0414
ECM (6%)						
Agt	Angiotensinogen (serpin peptidase inhibitor, clade A, member 8)	1387811_at	0.776	0.0268	0.542	0.0268
Serpine1	Serine (or cysteine) proteinase inhibitor, member 1	1392264_s_at	1.826	0.0457	3.244	0.0457
Serping1	Serine (or cysteine) proteinase inhibitor, clade G (C1 inhibitor), member 1 (angioedema, hereditary)	1372254_at	1.9	0.0207	2.274	0.0207
Slpi	Secretory leukocyte protease inhibitor	1367998_at	10.61	0.00124	45.6	0.00124
Slamf9_predicted	Similar to CD2 antigen family, member 10	1378443_at	4.37	0.0129	9.72	0.0129
Timp1	Tissue inhibitor of metalloproteinase 1	1367712_at	1.885	0.0392	3.231	0.0392
Growth related (7%)						
Igf1	Rat insulin-like growth factor I mRNA, 3′ end of mRNA	1388469_at	0.654	0.0191	0.331	0.0191
Igf1	Rat insulin-like growth factor I mRNA, 3′ end of mRNA	1382599_at	0.709	0.00887	0.279	0.00887
Il1b	Interleukin 1 beta	1398256_at	1.321	0.0248	9.51	0.0248
Nrp	Neuropilin	1373577_at	0.788	0.0287	0.594	0.0287
Tbrg1	Transforming growth factor beta regulated gene 1 (predicted)	1371509_at	1.249	0.0202	1.239	0.0202
Tnfsf4	Tumour necrosis factor (ligand) superfamily, member 4	1369481_at	0.61	0.00881	0.296	0.00881
Tnfrsf1b	Tumour necrosis factor receptor superfamily, member 1b	1392731_at	1.848	0.035	3.867	0.035
GTPase transduction (8%)						
Akt2	RAC protein kinase beta	1388765_at	0.725	0.0255	0.69	0.0255
Rapgef3	Rap guanine nucleotide exchange factor (GEF) 3	1368660_at	0.821	0.0305	0.564	0.0305
Rac2	Rac2_predicted	1372404_at	2.709	0.0348	4.414	0.0348
Iqgap3_predicted	IQ motif containing GTPase-activating protein 3 (predicted)	1374902_at	1.389	0.0407	1.865	0.0407
Rheb	Ras homologue enriched in brain	1375360_at	0.707	0.00627	0.276	0.00627
Myrip	Myosin VIIA and Rab interacting protein	1384095_at	0.807	0.00836	0.686	0.00836
Rasgrp3_predicted	RAS, guanyl-releasing protein 3 (predicted)	1390159_at	0.504	0.0462	0.299	0.0462
Arhgap21_predicted	Rho GTPase-activating protein 21 (predicted)	1378666_at	0.686	0.00507	0.677	0.00507
Ehd1_predicted	EH-domain containing 1	1372317_at	1.858	0.0146	3.482	0.0146
Immune complement pathway (4%)						
Cfb	B-factor, properdin	1389470_at	7.564	0.00304	17.23	0.00304
C2	Complement component 2	1383391_a_at	1.9	0.0186	2.713	0.0186
Daf1	Decay accelerating factor 1	1387951_at	0.466	0.0463	0.519	0.0463
C1r_predicted	Complement component 1, r subcomponent (predicted)	1383241_at	1.284	0.0201	1.79	0.0201
Immune response (12%)						
Saa3_predicted	Serum amyloid A 3 (predicted)	1392647_at	60.94	0.0137	149.4	0.0137
Dcir1/Clecsf6	Dendritic cell inhibitory receptor 1	1382153_at	2.162	0.0284	4.561	0.0284
Lyz	Lysozyme	1370154_at	1.44	0.0447	2.844	0.0447
Gbp2	Guanylate-binding protein 2, interferon-inducible	1368332_at	2.553	0.0206	7.9	0.0206
Cxcl11	Chemokine (C-X-C motif) ligand 11	1379365_at	3.568	0.0215	7.644	0.0215
Ltb	Lymphotoxin B	1379499_at	1.688	0.0206	2.77	0.0206
Pdcd1lg1_predicted	Programmed cell death 1 ligand 1 (predicted)	1382603_at	1.691	0.02	3.327	0.02
Ltc4s	Leukotriene C4 synthase	1387438_at	0.477	0.0117	0.194	0.0117
RT1-Aw2	RT1 class Ib, locus Aw2	1388071_x_at	1.348	0.0436	1.785	0.0436

TABLE 2. (Continued)

Gene symbol	Gene name	Accession number	11C7 Fold change	11C7 *P*-value	7B12 Fold change	7B12 *P*-value
Dcir4 / Clec4a1	Dendritic cell inhibitory receptor 4	1395003_at	2.733	0.0168	5.161	0.0168
Gp49b	Glycoprotein 49b	1375917_at	1.99	0.0396	3.749	0.0396
Dcir3	Dendritic cell inhibitory receptor 3	1389553_at	2.875	0.00929	5.483	0.00929
Lamp1	Lysosomal membrane glycoprotein 1	1375629_at	1.233	0.0458	1.807	0.0458
Inflammation (1%)						
Ncf1	Neutrophil cytosolic factor 1	1387413_at	1.471	0.0328	4.482	0.0328
Metabolism (2%)						
Car8	Carbonic anhydrase 8	1398431_at	1.358	0.0303	0.781	0.0303
Mell1_predicted	Similar to neprilysin (EC 3.4.24.11) II – rat (LOC313755), mRNA	1384748_at	0.361	0.0294	0.419	0.0294
Neurogenesis (3%)						
Dab2	Disabled homologue 2 (Drosophila)	1368202_a_at	1.592	0.0214	2.629	0.0214
Dab2	Disabled homologue 2 (Drosophila)	1372031_at	1.702	0.0298	2.265	0.0298
Kidins220	Kinase D-interacting substance of 220 kDa	1398311_a_at	0.727	0.0387	0.815	0.0387
Neurotransmission (3%)						
Cnga2	Cyclic nucleotide-gated channel 4	1387699_at	4.605	0.0431	2.821	0.0431
Egr1	Early growth response 1	1368321_at	0.758	0.0393	0.79	0.0393
Slc6a12	GABA transporter	1387295_at	1.278	0.0309	3.505	0.0309
Other (24%)						
MGC72612	Similar to expressed sequence AI449175	1382113_at	1.473	0.0277	0.728	0.0277
RGD1562732_predicted	Similar to glutathione *S*-transferase, theta 3	1371942_at	0.832	0.0447	0.658	0.0447
Lrrc46	Leucine-rich repeat containing 46	1375076_at	0.781	0.0215	0.652	0.0215
RGD1564982_predicted	Hypothetical LOC308556	1375464_at	1.483	0.00019	1.742	0.000194
RGD1565602_predicted	Similar to PLU1 (predicted)	1376347_at	0.831	0.0294	0.809	0.0294
RGD1311517_predicted	Similar to RIKEN cDNA 9430015G10	1378750_at	0.576	0.0225	1.384	0.0225
RGD1559748_predicted	Similar to palate lung and nasal carcinoma-like protein precursor (tongue plunc-like protein) (predicted)	1383203_at	1.351	0.0338	0.661	0.0338
RGD1565895_predicted	Similar to DRE1 protein (predicted)	1385499_at	0.572	0.0457	0.465	0.0457
Ifitm3	Interferon-induced transmembrane protein 3	1387995_a_at	1.534	0.0456	2.093	0.0456
Adfp	Adipose differentiation-related protein	1390383_at	1.591	0.00215	1.558	0.00215
Best5	Best5 protein	1370913_at	2.027	0.00017	6.885	0.000171
RGD1310066	Similar to mKIAA1002 protein (LOC362894)	1373814_at	0.777	0.0147	1.335	0.0147
RGD1305820_predicted	Similar to KIAA1337 protein (LOC313705)	1379955_at	0.569	0.0497	0.688	0.0497
RGD1305235_predicted	Similar to RIKEN cDNA 1700052N19 (LOC292267)	1385741_at	0.774	0.0115	0.797	0.0115
Sertad1	Similar to p34SEI-1 (LOC361526), mRNA	1372417_at	1.308	0.00414	1.237	0.00414
Asahl_predicted	*N*-acylsphingosine amidohydrolase (acid ceramidase)-like (predicted)	1390472_at	2.468	0.0116	4.772	0.0116
Tmem106a	Similar to hypothetical protein MGC37887 (predicted)	1374948_at	1.977	0.0295	3.422	0.0295
RGD1304816_predicted	Similar to mKIAA0674 protein (predicted)	1384616_at	2.177	0.0298	2.404	0.0298
RGD1559588_predicted	Similar to cell surface receptor FDFACT (predicted)	1385047_x_at	3.553	0.0174	6.655	0.0174
RGD1561144_predicted	Similar to *N*-acetylglucosamine 6-*O*-sulphotransferase (predicted)	1392444_at	1.248	0.0213	0.733	0.0213
RGD1559588_predicted	Similar to cell surface receptor FDFACT (predicted)	1393688_at	2.731	0.0163	5.974	0.0163
–	–	1396049_x_at	0.792	0.0416	0.434	0.0416
LOC288568	Similar to paired immunoglobulin-like type 2 receptor alpha	1398589_at	9.641	0.0346	25.91	0.0346
RGD1564403_predicted	Similar to leucine-rich repeat and sterile alpha motif containing 1	1396668_at	0.176	0.00281	0.107	0.00281
–	Similar to proline dehydrogenase; PRODH (LOC287950), mRNA	1372920_at	0.651	0.0244	0.656	0.0244
Upk3b_predicted	Similar to uroplakin IIIb (predicted)	1383460_at	1.435	0.00151	3.616	0.00151
Protein biosynthesis and modification (3%)						
Rpl39	Ribosomal protein L39	1367934_at	1.269	0.0135	1.84	0.0135
RGD1310265_predicted	Similar to alpha-1,4-*N*-acetylglucosaminyltransferase (Alpha4GnT) (predicted)	1393701_at	1.273	0.0302	1.269	0.0302
Tufm_predicted	Tu translation elongation factor, mitochondrial (predicted)	1395647_at	0.595	0.0114	0.525	0.0114
Proteolysis (2%)						
Ubap2_predicted	Ubiquitin-associated protein 2 (predicted)	1372127_at	1.37	0.0158	1.255	0.0158
Sod2	Superoxide dismutase2	1370173_at	2.051	0.0349	4.114	0.0349
Receptor (1%)						
Folr2_predicted	Similar to folate-binding protein 2 precursor – mouse (LOC293154), mRNA	1390348_at	3.026	0.00896	5.643	0.00896

TABLE 2. (Continued)

Gene symbol	Gene name	Accession number	11C7 Fold change	11C7 *P*-value	7B12 Fold change	7B12 *P*-value
RNA processing (1%)						
Exosc2_predicted	Exosome component 2 (predicted)	1379348_at	1.256	0.0386	1.298	0.0386
Sex differences (1%)						
Spag9_predicted	Sperm-associated antigen 9 (predicted)	1394436_at	0.816	0.0308	0.811	0.0308
Signalling (2%)						
Ms4a7_predicted	Similar to RIKEN cDNA A430103C15 (LOC293744), mRNA	1378193_at	4.955	0.0115	8.892	0.0115
Ppp1r14c	Protein phosphatase 1, regulatory (inhibitor) subunit 14c	1368716_at	0.713	0.0486	0.629	0.0486
Transcription (6%)						
Cbx1_predicted	Chromobox homologue 1 (Drosophila HP1 beta) (predicted)	1385157_at	1.301	0.0408	1.257	0.0408
Maf	V-maf musculoaponeurotic fibrosarcoma oncogene homologue (avian)	1387165_at	1.478	0.0494	2.648	0.0494
Arid1a_predicted	AT-rich interactive domain 1A (Swi1 like) (predicted)	1389850_at	1.329	0.0466	1.414	0.0466
Catsper2_predicted	Cation channel, sperm-associated 2	1391231_at	0.607	0.0463	0.589	0.0463
Whsc1l1_predicted	Wolf-Hirschhorn syndrome candidate 1-like 1 (predicted)	1394868_at	1.578	0.0439	1.494	0.0439
Nfkbiz_predicted	Nuclear factor of kappa light polypeptide gene enhancer in B-cells inhibitor, zeta (predicted)	1378032_at	1.85	0.0332	3.57	0.0332
Transport (4%)						
Cp	Ceruloplasmin	1368418_a_at	1.378	0.032	0.679	0.032
Fxyd2	FXYD domain-containing ion transport regulator 2	1387799_at	3.352	0.0416	10.99	0.0416
Slc27a4_predicted	Solute carrier family 27 (fatty acid transporter), member 4	1381263_at	1.6	0.0283	1.222	0.0283
Slc25a15_predicted	Solute carrier family 25 (mitochondrial carrier; ornithine transporter) member 15	1393947_at	1.23	0.00302	0.731	0.00302

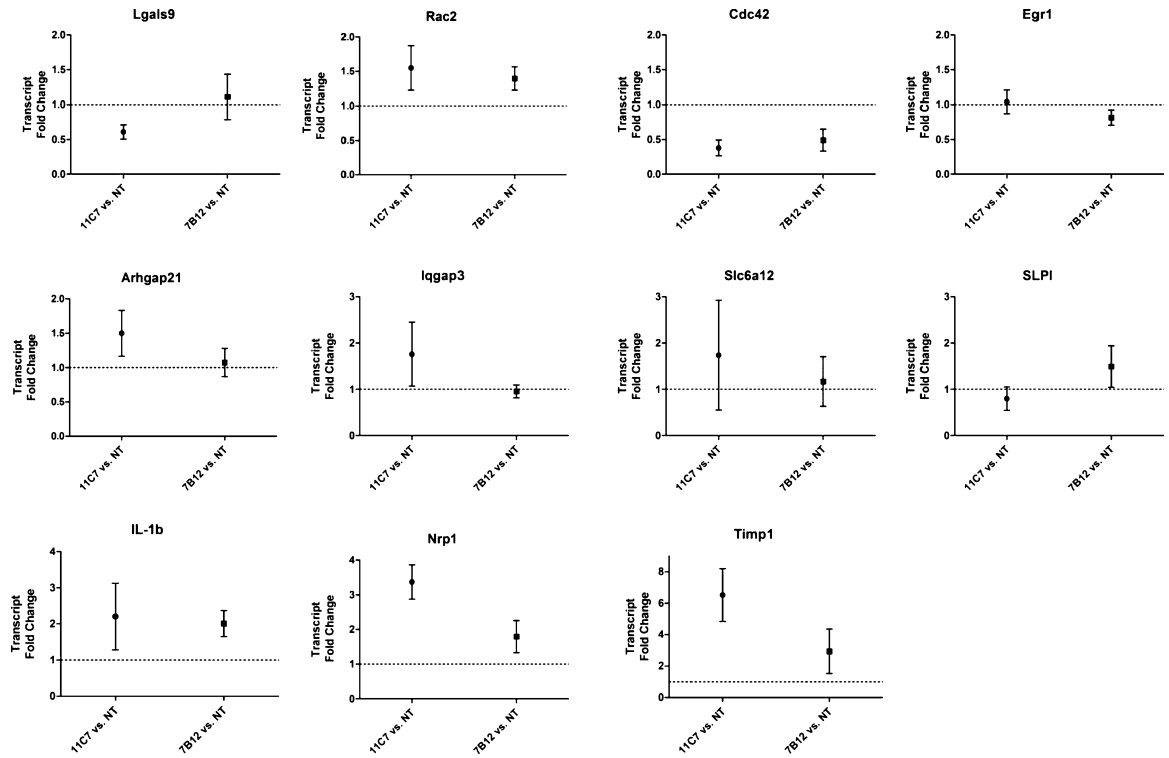

FIG. 8. qRT-PCR transcript validation plots. Ten genes, with the addition of Cdc42, were chosen for validation of the changes detected by the DNA microarray. The plots represent mean transcript fold changes of the anti-Nogo-A antibody treatment (11C7 and 7B12) compared with the NT cultures. Twenty-four cultures were pooled per treatment per replicate and three biological replicates were used. Error bars represent the SEM. Note that some genes have a high variability and there are some differences in the transcript fold changes, where the 11C7 treatment seems to give rise to stronger changes (contrary to what was observed with the microarray).

NF68-positive fibres we observed, without changes in MAP2a/b fibre density, suggests that in our model the increase in growth would be mainly axonal. This increase in the number of NF68-positive fibres may be due to the formation of new fibres or to an increased expression of this protein in pre-existing ones, previously below detection levels. In this later case, this increased expression would probably indicate axial growth. Axonal calibre is determined by axial growth, a process for which NF68 plays a crucial role (Hoffman *et al.*, 1987; Hoffman, 1988).

Organotypic hippocampal cultures lack external afferent input but form intrinsic circuitry very similar to the *in vivo* situation (Holopainen, 2005). Aberrant sprouting has been described during culture maturation mainly in the dentate gyrus both from collaterals (Coltman *et al.*, 1995) and from CA3 pyramidal cells (Sakaguchi *et al.*, 1994). There have been reports of hyperexcitability for different types of hippocampal neurons (McBain *et al.*, 1989; Streit *et al.*, 1989; Muller *et al.*, 1993). However, despite the observed evidence of axonal growth/sprouting, we have not been able to observe any indication of epileptic activity, neither spontaneous nor induced by repeated electrical stimulations, following anti-Nogo-A antibody treatment. One possible explanation could be that the observed elevation of the vesicular GABA transporter (Table 2) reflects an enhanced GABAergic inhibitory control following Nogo-A neutralization.

Changes at the mRNA level induced by Nogo-A neutralization

Previous studies have shown that Nogo-A signalling activates the family of small Rho GTPases (Niederost *et al.*, 2002; Fournier *et al.*, 2003; Schweigreiter *et al.*, 2004; Hsieh *et al.*, 2006; McKerracher & Higuchi, 2006). Our transcriptomic results confirmed the importance of this pathway in mediating Nogo-A neutralization effects. The members of the family of small Rho GTPases and their regulators were one of the most prominent categories of signalling molecules influenced by the neutralization of Nogo-A (Table 2 and Fig. 7). In particular, we observed changes in Arhgap21 and Iqgap3, key regulators of the family of small Rho GTPases and already known to be involved in neuronal growth responses (Dubois & Chavrier, 2005; Menetrey *et al.*, 2007; Wang *et al.*, 2007). Our results speak for their possible involvement in the regulation of the neuronal growth machinery, which we observed following antibody-mediated Nogo-A neutralization. mRNA levels of Arhgap21 (also known as Arhgap10; Menetrey *et al.*, 2007) were shown to be downregulated in the microarray analysis (11C7 = 0.686; 7B12 = 0.677 normalized to NT = 1.0) but upregulated by qRT-PCR (11C7 = 1.499; 7B12 = 1.073) after Nogo-A neutralization. Due to the possibility of false positives in the microarray approach and the higher precision/sensitivity of qRT-PCR, this latest result might better reflect the real expression level of this transcript. Arhgap21 is a known Cdc42-activating protein involved in the regulation of the actin cytoskeleton (Dubois & Chavrier, 2005) and also interacts with RhoA to hydrolyse and inactivate the GTP bound, active form (Sousa *et al.*, 2005). Therefore, we could speculate that its upregulation could be responsible for a decrease in RhoA activation, which could then translate into the observed enhancement of the neuronal growth machinery. However, due to the contradictory results obtained with distinct techniques, additional experiments, e.g. immunoblotting or immunohistochemistry, would be required to further clarify the role played by this candidate on a protein level. Contrary to Arhgap21, the upregulation of Iqgap3 found in our genomic approach (11C7 = 1.389) was confirmed by qRT-PCR (11C7 = 1.759) for the 11C7 treatment. At the protein level, Iqgap3 is a Rac1 and Cdc42 effector playing a pivotal role in neurite outgrowth (Wang *et al.*, 2007). Blocking Nogo-A also caused an upregulation in the expression level of Rac2 (11C7 = 2.709; 7B12 = 4.414), which was confirmed by qRT-PCR (11C7 = 1.549; 7B12 = 1.396) and has already been suggested to be involved in Nogo-A downstream signalling (Niederost *et al.*, 2002). All together, these changes indicate that complex regulatory signalling mechanisms, known to be able to affect neuronal cytoskeleton dynamics, are modulated by Nogo-A neutralization and might be involved in the observed regulation of the axonal growth response.

This regulation was reflected by the fact that also several trophic factors and other transcripts known to be involved in growth processes were found to be influenced by Nogo-A neutralization. TIMP-1 was described to be continuously but weakly expressed in pyramidal and granular cells of the hippocampus after birth and also be involved in neuroprotection, inhibiting excitotoxic cell death of neurons (Gardner & Ghorpade, 2003). It also has growth factor activity and is positively regulated by IL1β (Gardner & Ghorpade, 2003). Interestingly, in our approach we found both the mRNA levels of TIMP-1 (11C7 = 1.885; 7B12 = 3.231) and IL1β (11C7 = 1.321; 7B12 = 9.510) being upregulated after 5 days of anti-Nogo-A antibody treatment in intact mature cultures. Both changes were confirmed by qRT-PCR (TIMP-1: 11C7 = 6.610; 7B12 = 2.940; IL1β: 11C7 = 2.204; 7B12 = 2.008). The effects of IL1 in the lesioned CNS are controversial, ranging from *in vivo* evidence of worsened ischaemic lesion outcome to *in vitro* neuroprotective, neurotrophic and neurite outgrowth properties at low concentrations (nM–mM), or neurotoxic effects at higher concentrations (mM) after long exposure (Rothwell & Strijbos, 1995). Naturally expressed in the hippocampus at low amounts, an increased expression within physiological levels of IL1 could contribute to the observed outgrowth, as IL1β has also been shown to induce the expression of NF68 in human neuronal cells (Rempel *et al.*, 2001). IL1β could also contribute to the lack of epileptic activity due to its potentiation of GABA effects by enhancing conductance of Cl^- and inhibition of Ca^{2+} currents in hippocampal neurons (Rothwell & Hopkins, 1995).

Other immune response-related proteins are Galectins. The most well-known member of this family is Galectin-1 with both anti- and pro-inflammatory properties (Toscano *et al.*, 2007). Interestingly, like cytokines and interleukins, Galectin-1 has been shown to promote peripheral nerve fibre growth when oxidized (Horie *et al.*, 2005; Kadoya & Horie, 2005). The transcripts of Galectin-5 and -9 were both found to be upregulated after Nogo-A neutralization in intact mature cultures in our transcriptomic screening. However, these changes were not confirmed by qRT-PCR.

A very interesting candidate gene, whose upregulation following 7B12 treatment was confirmed by qRT-PCR, is SLPI, the second highest upregulated transcript in microarray analysis. Most recently, SLPI was shown to overcome myelin-associated glycoprotein (MAG)-induced neurite outgrowth inhibition (Filbin, M.T. personal communication). SLPI has also been described to be involved in neuroprotection from stroke and ischaemia (Wang *et al.*, 2003; Feuerstein, 2006). Furthermore, it is a target of epidermal growth factor (Velarde *et al.*, 2005) and a type 1 insulin-like growth factor receptor-regulated protein (Wang *et al.*, 2006). In our screening, SLPI was shown to be upregulated 10.61- and 45.6-fold after 5 days of treatment with anti-Nogo-A antibodies (11C7 and 7B12, respectively). The qRT-PCR approach confirmed the upregulation of SLPI following 7B12 treatment (7B12 = 1.493), even if at a smaller order of magnitude. Further experiments would be needed to explore the possibility that SLPI could be a strong candidate for overcoming different myelin-associated neurite outgrowth inhibitory molecules, e.g. MAG and Nogo-A.

As previously mentioned, differences between microarray and qRT-PCR data were observed. Out of the list of genes we chose to validate, only 50% or 60% of the transcripts were confirmed for 11C7 or 7B12, respectively. Although several studies have shown high correlation between their microarray and qRT-PCR validation data (Dallas *et al.*, 2005; Koscielny *et al.*, 2005; Michiels *et al.*, 2007), we believe that the expectation of the same magnitude of changes in the two approaches would be somewhat unrealistic. Even if it could be argued that when using the same experimental sample for validation the correlation between the two techniques should be high (Michiels *et al.*, 2007), some experts believe that using the same experimental sample for validation does not actually constitute a validation (Allison *et al.*, 2006; Michiels *et al.*, 2007), and that independent experimental and eventually biological samples should be tested. In accordance with this opinion, for qRT-PCR validation we processed total RNA extracted from an independent set of cultures, which therefore represented separate experimental and biological samples. This approach clearly introduces higher variability in the data, which relates mainly to biological differences as several cultures were pooled in order to reduce individual experimental variability and favour changes common to the sampled population.

In addition, in order not to miss biologically relevant gene changes we did not further restrict our microarray data by performing multiple testing analyses, which clearly results in a type I error or the increase in false positive discovery (Ransohoff, 2005). This increased false positive error probability could account for the higher number of observed discrepancies between the microarray data and the subsequent qRT-PCR validation.

It should also be pointed out that probes designed for qRT-PCR experiments are not the same as for microarray experiments, and that it has been already argued that poor correlations between microarray and qRT-PCR data can be due to different subsets of alternative transcripts that may be recognized by microarray and qRT-PCR probes, to the existence of cross-hybridizing transcripts differentially recognized by the oligonucleotide probe sets and qRT-PCR probes, to gene-specific variation related to the different hybridization kinetics associated with the two techniques, and to misleading results associated with errors in GeneBank sequence data and/or probe set annotations (Dallas *et al.*, 2005). Overall, despite the observed discrepancies, we are confident that those genes for which we were able to validate changes by qRT-PCR or by additional techniques, e.g. immunohistochemistry, point to an increased growth response on the molecular level following Nogo-A neutralization.

Nogo-A localization

Whether the growth response induced by the specific function-blocking anti-Nogo-A antibodies is due to interference with oligodendrocyte, or neuronal Nogo-A, or both, remains unanswered. Several studies on spinal cord injury in adult rats and monkeys have shown that blockade of Nogo-A or its receptor complex allows axons to sprout and regenerate beyond the lesion site (Yiu & He, 2003; He & Koprivica, 2004; Schwab, 2004). The enhanced growth response in the hippocampal tissue could be due to the neutralization of an inhibitory signal from the oligodendrocytes to the neurons. Such a signal could physiologically function in the intact adult CNS to restrict growth in order to stabilize the network after differentiation. We cannot exclude, however, that the effects observed could also be at least partially due to neuronal Nogo-A neutralization, as neuronal Nogo-A has also been shown to potentially affect neurite growth both during development and in adulthood (Montani L., personal communication), although the function of neuronal Nogo-A in the hippocampus is not yet understood.

In conclusion, we show that Nogo-A neutralization induces axonal growth/sprouting in both lesioned and non-lesioned differentiated organotypic hippocampal slice cultures. This demonstrates the importance of Nogo-A as a negative regulator of growth and plasticity in the adult CNS. The lack of observable epileptic activity after treatment with Nogo-A-specific antibodies suggests that fibre growth induced by Nogo-A neutralization may not be random or chaotic. This is in line with a previous observation of no enhancement in pain perception threshold *in vivo* in animals treated with anti Nogo-A antibodies following spinal cord injuries (Merkler *et al.*, 2001; Liebscher *et al.*, 2005; Freund *et al.*, 2006). Guidance and target recognition signals may still be present in the tissue, and activity-dependent mechanisms may control synapse stabilization and axon branch survival (Maier & Schwab, 2006). The increased growth capacity of the neurons reflected by the regulation of small Rho-GTPases signalling pathways, growth factors and early growth cytoskeletal markers (i.e. Gap43 and NF68) in response to neuronal Nogo-A neutralization and the decreased growth inhibitory properties of the CNS tissue due to myelin Nogo-A neutralization are probably responsible for the enhanced growth/sprouting and regeneration responses observed in our study, as well as in many studies following spinal cord or brain injuries and subsequent Nogo-A neutralization.

Supporting information

Additional supporting information may be found in the online version of this article:

Table S1. Gene expression changes induced by 11C7 anti-Nogo-A antibody only.

Table S2. Gene expression changes induced by 7B12 anti-Nogo-A antibody only.

Table S3. Gene expression changes common to 11C7 and IgG treatments.

Table S4. Gene expression changes common to 7B12 and IgG treatments.

Table S5. Gene expression changes induce by IgG control antibody only.

Table S6. Gene expression changes common to all treatments.

Please note: Wiley-Blackwell are not responsible for the content or functionality of any supporting materials supplied by the authors. Any queries (other than missing material) should be directed to the corresponding author for the article.

Acknowledgements

We thank Andrea Patrignani from the Functional Genomics Center Zurich for expert assistance with the genomics experiments, Lotty Rietschin for patient training in the establishment of the slice culture system, Dr R.A. McKinney for talented supervision and insight into confocal imaging and advice, Dr Ralf Horres from GenXpro for the qRT-PCR experiments and Roland Schoeb for the graphic work. This work has been supported by the Swiss National Foundation, the Swiss National Centre of Competence in Research, the Portuguese Fundação para a Ciência e Tecnologia and the GABBA PhD program in Porto, Portugal.

Abbreviations

Arhgap21, Rho GTPase-activating protein 21; DIV, days *in vitro;* ECM, extracellular array; GABA, γ-aminobutyric acid; Gap43, growth-associated protein 43; Iqgap3, IQ motif containing GTPase-activating protein 3; MAG, myelin-associated glycoprotein; MAP2a/b, microtubule-associated protein 2a/b; MEA, multi-electrode array; NF68, neurofilament 68; NT, non-treated; qRT-PCR, quantitative real-time polymerase chain reaction; SDS, sodium dodecyl sulphate; Slc6a12, vesicular GABA transporter; SLPI, secretory leukocyte protease inhibitor; TIMP-1, tissue inhibitor of metalloproteinase.

References

Allison, D.B., Cui, X., Page, G.P. & Sabripour, M. (2006) Microarray data analysis: from disarray to consolidation and consensus. *Nat Rev Genet*, **7**, 55–65.

Bahr, B.A. (1995) Long-term hippocampal slices: a model system for investigating synaptic mechanisms and pathologic processes. *J. Neurosci. Res.*, **42**, 294–305.

Bareyre, F.M., Haudenschild, B. & Schwab, M.E. (2002) Long-lasting sprouting and gene expression changes induced by the monoclonal antibody IN-1 in the adult spinal cord. *J. Neurosci.*, **22**, 7097–7110.

Benowitz, L.I. & Yin, Y. (2007) Combinatorial treatments for promoting axon regeneration in the CNS: strategies for overcoming inhibitory signals and activating neurons' intrinsic growth state. *Dev. Neurobiol.*, **67**, 1148–1165.

Berger, T. & Frotscher, M. (1994) Distribution and morphological characteristics of oligodendrocytes in the rat hippocampus in situ and in vitro: an immunocytochemical study with the monoclonal Rip antibody. *J. Neurocytol.*, **23**, 61–74.

Buffo, A., Zagrebelsky, M., Huber, A.B., Skerra, A., Schwab, M.E., Strata, P. & Rossi, F. (2000) Application of neutralizing antibodies against NI-35/250 myelin-associated neurite growth inhibitory proteins to the adult rat cerebellum induces sprouting of uninjured purkinje cell axons. *J. Neurosci.*, **20**, 2275–2286.

Caroni, P. & Schwab, M.E. (1988) Two membrane protein fractions from rat central myelin with inhibitory properties for neurite growth and fibroblast spreading. *J. Cell Biol.*, **106**, 1281–1288.

Chen, M.S., Huber, A.B., van der Haar, M.E., Frank, M., Schnell, L., Spillmann, A.A., Christ, F. & Schwab, M.E. (2000) Nogo-A is a myelin-associated neurite outgrowth inhibitor and an antigen for monoclonal antibody IN-1. *Nature*, **403**, 434–439.

Coltman, B.W., Earley, E.M., Shahar, A., Dudek, F.E. & Ide, C.F. (1995) Factors influencing mossy fiber collateral sprouting in organotypic slice cultures of neonatal mouse hippocampus. *J. Comp. Neurol.*, **362**, 209–222.

Dallas, P.B., Gottardo, N.G., Firth, M.J., Beesley, A.H., Hoffmann, K., Terry, P.A., Freitas, J.R., Boag, J.M., Cummings, A.J. & Kees, U.R. (2005) Gene expression levels assessed by oligonucleotide microarray analysis and quantitative real-time RT-PCR – how well do they correlate? *BMC Genomics*, **6**, 59.

Dimou, L., Schnell, L., Montani, L., Duncan, C., Simonen, M., Schneider, R., Liebscher, T., Gullo, M. & Schwab, M.E. (2006) Nogo-A-deficient mice reveal strain-dependent differences in axonal regeneration. *J. Neurosci.*, **26**, 5591–5603.

Dodd, D.A., Niederoest, B., Bloechlinger, S., Dupuis, L., Loeffler, J.P. & Schwab, M.E. (2005) Nogo-A, -B, and -C are found on the cell surface and interact together in many different cell types. *J. Biol. Chem.*, **280**, 12494–12502.

Dubois, T. & Chavrier, P. (2005) ARHGAP10, a novel RhoGAP at the cross-road between ARF1 and Cdc42 pathways, regulates Arp2/3 complex and actin dynamics on Golgi membranes. *Med. Sci. (Paris)*, **21**, 692–694.

Emerick, A.J., Neafsey, E.J., Schwab, M.E. & Kartje, G.L. (2003) Functional reorganization of the motor cortex in adult rats after cortical lesion and treatment with monoclonal antibody IN-1. *J. Neurosci.*, **23**, 4826–4830.

Feuerstein, G. (2006) Inflammation and stroke: therapeutic effects of adenoviral expression of secretory leukocyte protease inhibitor. *Front Biosci.*, **11**, 1750–1757.

Filbin, M.T. (2006) Recapitulate development to promote axonal regeneration: good or bad approach? *Philos. Trans. R. Soc. Lond. B Biol. Sci.*, **361**, 1565–1574.

Fournier, A.E., GrandPre, T. & Strittmatter, S.M. (2001) Identification of a receptor mediating Nogo-66 inhibition of axonal regeneration. *Nature*, **409**, 341–346.

Fournier, A.E., Takizawa, B.T. & Strittmatter, S.M. (2003) Rho kinase inhibition enhances axonal regeneration in the injured CNS. *J. Neurosci.*, **23**, 1416–1423.

Freund, P., Schmidlin, E., Wannier, T., Bloch, J., Mir, A., Schwab, M.E. & Rouiller, E.M. (2006) Nogo-A-specific antibody treatment enhances sprouting and functional recovery after cervical lesion in adult primates. *Nat. Med.*, **12**, 790–792.

Gahwiler, B.H. (1981a) Morphological differentiation of nerve cells in thin organotypic cultures derived from rat hippocampus and cerebellum. *Proc. R. Soc. Lond. B Biol. Sci.*, **211**, 287–290.

Gahwiler, B.H. (1981b) Nerve cells in organotypic cultures. *JAMA*, **245**, 1858–1859.

Gahwiler, B.H. (1981c) Organotypic monolayer cultures of nervous tissue. *J. Neurosci. Methods*, **4**, 329–342.

Gahwiler, B.H., Capogna, M., Debanne, D., McKinney, R.A. & Thompson, S.M. (1997) Organotypic slice cultures: a technique has come of age. *Trends Neurosci.*, **20**, 471–477.

Gardner, J. & Ghorpade, A. (2003) Tissue inhibitor of metalloproteinase (TIMP)-1: the TIMPed balance of matrix metalloproteinases in the central nervous system. *J. Neurosci. Res.*, **74**, 801–806.

Gianola, S., Savio, T., Schwab, M.E. & Rossi, F. (2003) Cell-autonomous mechanisms and myelin-associated factors contribute to the development of Purkinje axon intracortical plexus in the rat cerebellum. *J. Neurosci.*, **23**, 4613–4624.

Gil, V., Nicolas, O., Mingorance, A., Urena, J.M., Tang, B.L., Hirata, T., Saez-Valero, J., Ferrer, I., Soriano, E. & del Rio, J.A. (2006) Nogo-A expression in the human hippocampus in normal aging and in Alzheimer disease. *J. Neuropathol. Exp. Neurol.*, **65**, 433–444.

GrandPre, T., Li, S. & Strittmatter, S.M. (2002) Nogo-66 receptor antagonist peptide promotes axonal regeneration. *Nature*, **417**, 547–551.

Hakkoum, D., Stoppini, L. & Muller, D. (2007) Interleukin-6 promotes sprouting and functional recovery in lesioned organotypic hippocampal slice cultures. *J. Neurochem.*, **100**, 747–757.

He, Z. & Koprivica, V. (2004) The Nogo signaling pathway for regeneration block. *Annu. Rev. Neurosci.*, **27**, 341–368.

Hoffman, P.N. (1988) Distinct roles of neurofilament and tubulin gene expression in axonal growth. *Ciba Found. Symp.*, **138**, 192–204.

Hoffman, P.N., Cleveland, D.W., Griffin, J.W., Landes, P.W., Cowan, N.J. & Price, D.L. (1987) Neurofilament gene expression: a major determinant of axonal caliber. *Proc. Natl Acad. Sci. USA*, **84**, 3472–3476.

Holopainen, I.E. (2005) Organotypic hippocampal slice cultures: a model system to study basic cellular and molecular mechanisms of neuronal cell death, neuroprotection, and synaptic plasticity. *Neurochem. Res.*, **30**, 1521–1528.

Horie, H., Kadoya, T., Sango, K. & Hasegawa, M. (2005) Oxidized galectin-1 is an essential factor for peripheral nerve regeneration. *Curr. Drug Targets*, **6**, 385–394.

Hsieh, S.H., Ferraro, G.B. & Fournier, A.E. (2006) Myelin-associated inhibitors regulate cofilin phosphorylation and neuronal inhibition through LIM kinase and Slingshot phosphatase. *J. Neurosci.*, **26**, 1006–1015.

Huber, A.B., Weinmann, O., Brosamle, C., Oertle, T. & Schwab, M.E. (2002) Patterns of Nogo mRNA and protein expression in the developing and adult rat and after CNS lesions. *J. Neurosci.*, **22**, 3553–3567.

Kadoya, T. & Horie, H. (2005) Structural and functional studies of galectin-1: a novel axonal regeneration-promoting activity for oxidized galectin-1. *Curr. Drug Targets*, **6**, 375–383.

Kim, J.E., Li, S., GrandPre, T., Qiu, D. & Strittmatter, S.M. (2003) Axon regeneration in young adult mice lacking Nogo-A/B. *Neuron*, **38**, 187–199.

Kim, J.E., Liu, B.P., Park, J.H. & Strittmatter, S.M. (2004) Nogo-66 receptor prevents raphespinal and rubrospinal axon regeneration and limits functional recovery from spinal cord injury. *Neuron*, **44**, 439–451.

Kleiman, R., Banker, G. & Steward, O. (1990) Differential subcellular localization of particular mRNAs in hippocampal neurons in culture. *Neuron*, **5**, 821–830.

Koscielny, S., Michiels, S., Boige, V. & Hill, C. (2005) Validation of microarray data by quantitative reverse-transcriptase polymerase chain reaction. *J. Clin. Oncol.*, **23**, 9439–9440; author reply 9440.

Lee, J.K., Kim, J.E., Sivula, M. & Strittmatter, S.M. (2004) Nogo receptor antagonism promotes stroke recovery by enhancing axonal plasticity. *J. Neurosci.*, **24**, 6209–6217.

Li, S., Liu, B.P., Budel, S., Li, M., Ji, B., Walus, L., Li, W., Jirik, A., Rabacchi, S., Choi, E., Worley, D., Sah, D.W., Pepinsky, B., Lee, D., Relton, J. & Strittmatter, S.M. (2004) Blockade of Nogo-66, myelin-associated glycoprotein, and oligodendrocyte myelin glycoprotein by soluble Nogo-66 receptor promotes axonal sprouting and recovery after spinal injury. *J. Neurosci.*, **24**, 10511–10520.

Liebscher, T., Schnell, L., Schnell, D., Scholl, J., Schneider, R., Gullo, M., Fouad, K., Mir, A., Rausch, M., Kindler, D., Hamers, F.P. & Schwab, M.E. (2005) Nogo-A antibody improves regeneration and locomotion of spinal cord-injured rats. *Ann. Neurol.*, **58**, 706–719.

Lind, D., Franken, S., Kappler, J., Jankowski, J. & Schilling, K. (2005) Characterization of the neuronal marker NeuN as a multiply phosphorylated antigen with discrete subcellular localization. *J. Neurosci. Res.*, **79**, 295–302.

Maier, I.C. & Schwab, M.E. (2006) Sprouting, regeneration and circuit formation in the injured spinal cord: factors and activity. *Philos. Trans. R. Soc. Lond. B Biol. Sci.*, **361**, 1611–1634.

McBain, C.J., Boden, P. & Hill, R.G. (1989) Rat hippocampal slices 'in vitro' display spontaneous epileptiform activity following long-term organotypic culture. *J. Neurosci. Methods*, **27**, 35–49.

McKerracher, L. & Higuchi, H. (2006) Targeting Rho to stimulate repair after spinal cord injury. *J. Neurotrauma*, **23**, 309–317.
McKinney, R.A., Debanne, D., Gahwiler, B.H. & Thompson, S.M. (1997) Lesion-induced axonal sprouting and hyperexcitability in the hippocampus in vitro: implications for the genesis of posttraumatic epilepsy. *Nat. Med.*, **3**, 990–996.
McKinney, R.A., Luthi, A., Bandtlow, C.E., Gahwiler, B.H. & Thompson, S.M. (1999) Selective glutamate receptor antagonists can induce or prevent axonal sprouting in rat hippocampal slice cultures. *Proc. Natl Acad. Sci. USA*, **96**, 11631–11636.
Meier, S., Brauer, A.U., Heimrich, B., Schwab, M.E., Nitsch, R. & Savaskan, N.E. (2003) Molecular analysis of Nogo expression in the hippocampus during development and following lesion and seizure. *FASEB J.*, **17**, 1153–1155.
Menetrey, J., Perderiset, M., Cicolari, J., Dubois, T., Elkhatib, N., Khadali, F.E., Franco, M., Chavrier, P. & Houdusse, A. (2007) Structural basis for ARF1-mediated recruitment of ARHGAP21 to Golgi membranes. *EMBO J.*, **26**, 1953–1962.
Merkler, D., Metz, G.A., Raineteau, O., Dietz, V., Schwab, M.E. & Fouad, K. (2001) Locomotor recovery in spinal cord-injured rats treated with an antibody neutralizing the myelin-associated neurite growth inhibitor Nogo-A. *J. Neurosci.*, **21**, 3665–3673.
Mi, S., Lee, X., Shao, Z., Thill, G., Ji, B., Relton, J., Levesque, M., Allaire, N., Perrin, S., Sands, B., Crowell, T., Cate, R.L., McCoy, J.M. & Pepinsky, R.B. (2004) LINGO-1 is a component of the Nogo-66 receptor/p75 signaling complex. *Nat. Neurosci.*, **7**, 221–228.
Michiels, S., Koscielny, S. & Hill, C. (2007) Interpretation of microarray data in cancer. *Br. J. Cancer*, **96**, 1155–1158.
Mielke, J.G., Comas, T., Woulfe, J., Monette, R., Chakravarthy, B. & Mealing, G.A. (2005) Cytoskeletal, synaptic, and nuclear protein changes associated with rat interface organotypic hippocampal slice culture development. *Brain Res. Dev. Brain Res.*, **160**, 275–286.
Mingorance, A., Sole, M., Muneton, V., Martinez, A., Nieto-Sampedro, M., Soriano, E. & del Rio, J.A. (2006) Regeneration of lesioned entorhino-hippocampal axons in vitro by combined degradation of inhibitory proteoglycans and blockade of Nogo-66/NgR signaling. *FASEB J.*, **20**, 491–493.
Mullen, R.J., Buck, C.R. & Smith, A.M. (1992) NeuN, a neuronal specific nuclear protein in vertebrates. *Development*, **116**, 201–211.
Muller, D., Buchs, P.A. & Stoppini, L. (1993) Time course of synaptic development in hippocampal organotypic cultures. *Brain Res. Dev. Brain Res.*, **71**, 93–100.
Niederost, B., Oertle, T., Fritsche, J., McKinney, R.A. & Bandtlow, C.E. (2002) Nogo-A and myelin-associated glycoprotein mediate neurite growth inhibition by antagonistic regulation of RhoA and Rac1. *J. Neurosci.*, **22**, 10368–10376.
Noraberg, J., Poulsen, F.R., Blaabjerg, M., Kristensen, B.W., Bonde, C., Montero, M., Meyer, M., Gramsbergen, J.B. & Zimmer, J. (2005) Organotypic hippocampal slice cultures for studies of brain damage, neuroprotection and neurorepair. *Curr. Drug Targets CNS Neurol Disord*, **4**, 435–452.
Oertle, T., van der Haar, M.E., Bandtlow, C.E., Robeva, A., Burfeind, P., Buss, A., Huber, A.B., Simonen, M., Schnell, L., Brosamle, C., Kaupmann, K., Vallon, R. & Schwab, M.E. (2003) Nogo-A inhibits neurite outgrowth and cell spreading with three discrete regions. *J. Neurosci.*, **23**, 5393–5406.
Papadopoulos, C.M., Tsai, S.Y., Alsbiei, T., O'Brien, T.E., Schwab, M.E. & Kartje, G.L. (2002) Functional recovery and neuroanatomical plasticity following middle cerebral artery occlusion and IN-1 antibody treatment in the adult rat. *Ann. Neurol.*, **51**, 433–441.
Papadopoulos, C.M., Tsai, S.Y., Cheatwood, J.L., Bollnow, M.R., Kolb, B.E., Schwab, M.E. & Kartje, G.L. (2006) Dendritic plasticity in the adult rat following middle cerebral artery occlusion and nogo-a neutralization. *Cereb. Cortex*, **16**, 529–536.
Park, J.B., Yiu, G., Kaneko, S., Wang, J., Chang, J., He, X.L., Garcia, K.C. & He, Z. (2005) A TNF receptor family member, TROY, is a coreceptor with Nogo receptor in mediating the inhibitory activity of myelin inhibitors. *Neuron*, **45**, 345–351.
Ransohoff, D.F. (2005) Bias as a threat to the validity of cancer molecular-marker research. *Nat. Rev. Cancer*, **5**, 142–149.
Reines, A., Cereseto, M., Ferrero, A., Bonavita, C. & Wikinski, S. (2004) Neuronal cytoskeletal alterations in an experimental model of depression. *Neuroscience*, **129**, 529–538.
Rempel, H., Kusdra, L. & Pulliam, L. (2001) Interleukin-1beta up-regulates expression of neurofilament light in human neuronal cells. *J. Neurochem.*, **78**, 640–645.
Rothwell, N.J. & Hopkins, S.J. (1995) Cytokines and the nervous system II: actions and mechanisms of action. *Trends Neurosci.*, **18**, 130–136.
Rothwell, N.J. & Strijbos, P.J. (1995) Cytokines in neurodegeneration and repair. *Int. J. Dev. Neurosci.*, **13**, 179–185.
Sakaguchi, T., Okada, M. & Kawasaki, K. (1994) Sprouting of CA3 pyramidal neurons to the dentate gyrus in rat hippocampal organotypic cultures. *Neurosci. Res.*, **20**, 157–164.
Schnell, L. & Schwab, M.E. (1990) Axonal regeneration in the rat spinal cord produced by an antibody against myelin-associated neurite growth inhibitors. *Nature*, **343**, 269–272.
Schwab, M.E. (2004) Nogo and axon regeneration. *Curr. Opin. Neurobiol.*, **14**, 118–124.
Schweigreiter, R., Walmsley, A.R., Niederost, B., Zimmermann, D.R., Oertle, T., Casademunt, E., Frentzel, S., Dechant, G., Mir, A. & Bandtlow, C.E. (2004) Versican V2 and the central inhibitory domain of Nogo-A inhibit neurite growth via p75NTR/NgR-independent pathways that converge at RhoA. *Mol. Cell. Neurosci.*, **27**, 163–174.
Shaw, G. & Weber, K. (1981) The distribution of the neurofilament triplet proteins within individual neurones. *Exp. Cell Res.*, **136**, 119–125.
Shaw, G., Banker, G.A. & Weber, K. (1985) An immunofluorescence study of neurofilament protein expression by developing hippocampal neurons in tissue culture. *Eur. J. Cell Biol.*, **39**, 205–216.
Simonen, M., Pedersen, V., Weinmann, O., Schnell, L., Buss, A., Ledermann, B., Christ, F., Sansig, G., van der Putten, H. & Schwab, M.E. (2003) Systemic deletion of the myelin-associated outgrowth inhibitor Nogo-A improves regenerative and plastic responses after spinal cord injury. *Neuron*, **38**, 201–211.
Sousa, S., Cabanes, D., Archambaud, C., Colland, F., Lemichez, E., Popoff, M., Boisson-Dupuis, S., Gouin, E., Lecuit, M., Legrain, P. & Cossart, P. (2005) ARHGAP10 is necessary for alpha-catenin recruitment at adherens junctions and for Listeria invasion. *Nat. Cell Biol.*, **7**, 954–960.
Stoppini, L., Buchs, P.A. & Muller, D. (1991) A simple method for organotypic cultures of nervous tissue. *J. Neurosci. Methods*, **37**, 173–182.
Stoppini, L., Buchs, P.A. & Muller, D. (1993) Lesion-induced neurite sprouting and synapse formation in hippocampal organotypic cultures. *Neuroscience*, **57**, 985–994.
Stoppini, L., Parisi, L., Oropesa, C. & Muller, D. (1997) Sprouting and functional recovery in co-cultures between old and young hippocampal organotypic slices. *Neuroscience*, **80**, 1127–1136.
Streit, P., Thompson, S.M. & Gahwiler, B.H. (1989) Anatomical and physiological properties of GABAergic neurotransmission in organotypic slice cultures of rat hippocampus. *Eur. J. Neurosci.*, **1**, 603–615.
Toscano, M.A., Ilarregui, J.M., Bianco, G.A., Campagna, L., Croci, D.O., Salatino, M. & Rabinovich, G.A. (2007) Dissecting the pathophysiologic role of endogenous lectins: glycan-binding proteins with cytokine-like activity? *Cytokine Growth Factor Rev.*, **18**, 57–71.
Trifunovski, A., Josephson, A., Bickford, P.C., Olson, L. & Brene, S. (2006) Selective decline of Nogo mRNA in the aging brain. *Neuroreport*, **17**, 913–916.
Velarde, M.C., Parisek, S.I., Eason, R.R., Simmen, F.A. & Simmen, R.C. (2005) The secretory leukocyte protease inhibitor gene is a target of epidermal growth factor receptor action in endometrial epithelial cells. *J. Endocrinol.*, **184**, 141–151.
Wang, K.C., Kim, J.A., Sivasankaran, R., Segal, R. & He, Z. (2002) P75 interacts with the Nogo receptor as a co-receptor for Nogo, MAG and OMgp. *Nature*, **420**, 74–78.
Wang, X., Li, X., Xu, L., Zhan, Y., Yaish-Ohad, S., Erhardt, J.A., Barone, F.C. & Feuerstein, G.Z. (2003) Up-regulation of secretory leukocyte protease inhibitor (SLPI) in the brain after ischemic stroke: adenoviral expression of SLPI protects brain from ischemic injury. *Mol. Pharmacol.*, **64**, 833–840.
Wang, N., Thuraisingam, T., Fallavollita, L., Ding, A., Radzioch, D. & Brodt, P. (2006) The secretory leukocyte protease inhibitor is a type 1 insulin-like growth factor receptor-regulated protein that protects against liver metastasis by attenuating the host proinflammatory response. *Cancer Res.*, **66**, 3062–3070.
Wang, S., Watanabe, T., Noritake, J., Fukata, M., Yoshimura, T., Itoh, N., Harada, T., Nakagawa, M., Matsuura, Y., Arimura, N. & Kaibuchi, K. (2007) IQGAP3, a novel effector of Rac1 and Cdc42, regulates neurite outgrowth. *J. Cell Sci.*, **120**, 567–577.
Wiessner, C., Bareyre, F.M., Allegrini, P.R., Mir, A.K., Frentzel, S., Zurini, M., Schnell, L., Oertle, T. & Schwab, M.E. (2003) Anti-Nogo-A antibody infusion 24 hours after experimental stroke improved behavioral outcome and corticospinal plasticity in normotensive and spontaneously hypertensive rats. *J. Cereb. Blood Flow Metab.*, **23**, 154–165.
Yiu, G. & He, Z. (2003) Signaling mechanisms of the myelin inhibitors of axon regeneration. *Curr. Opin. Neurobiol.*, **13**, 545–551.
Zagrebelsky, M., Buffo, A., Skerra, A., Schwab, M.E., Strata, P. & Rossi, F. (1998) Retrograde regulation of growth-associated gene expression in adult rat Purkinje cells by myelin-associated neurite growth inhibitory proteins. *J. Neurosci.*, **18**, 7912–7929.